

**STUDYING RESISTIVE SWITCHING BEHAVIOR IN
ZINC OXIDE NANOWIRES WITH ATOMIC FORCE
MICROSCOPE**



**A Thesis Submitted in Partial Fulfillment of the Requirements for the
Degree of Master of Science in Physics
Suranaree University of Technology
Academic Year 2018**

การศึกษาพฤติกรรมการเปลี่ยนลำดับค่าความต้านทานในเส้นลวด
นาโนซิงออกไซด์ด้วยกล้องจุลทรรศน์แรงอะตอม



นางสาวอรดี ศรีกิมแก้ว

วิทยานิพนธ์นี้เป็นส่วนหนึ่งของการศึกษาตามหลักสูตรปริญญาวิทยาศาสตรมหาบัณฑิต
สาขาวิชาฟิสิกส์
มหาวิทยาลัยเทคโนโลยีสุรนารี
ปีการศึกษา 2561

**STUDYING RESISTIVE SWITCHING BEHAVIOR IN ZINC
OXIDE NANOWIRES WITH ATOMIC FORCE MICROSCOPE**

Suranaree University of Technology has approved this thesis submitted in partial fulfillment of the requirements for a Master's Degree.

Thesis Examining Committee



(Dr. Nuanwan Sanguansak)

Chairperson



(Dr. Worasom Kundhikanjana)

Member (Thesis Advisor)



(Dr. Annop Klamchuen)

Member



(Assoc. Prof. Dr. Puangratana Pairor)

Member



(Prof. Dr. Santi Maensiri)

Vice Rector for Academic Affairs

and Internationalization



(Asst. Prof. Dr. Worawat Meevasana)

Dean of Institute of Science

อรรถิ ศรีกิมแก้ว : การศึกษาพฤติกรรมการเปลี่ยนกลับค่าความต้านทานในเส้นลวดนาโนซิงออกไซด์ด้วยกล้องจุลทรรศน์แรงอะตอม (STUDYING RESISTIVE SWITCHING BEHAVIOR IN ZINC OXIDE NANOWIRES WITH ATOMIC FORCE MICROSCOPE). อาจารย์ที่ปรึกษา : อาจารย์ ดร.วรสุม กุณทีกาญจน์, 48 หน้า.

การศึกษาปรากฏการณ์การเปลี่ยนกลับค่าความต้านทานเป็นสิ่งสำคัญสำหรับเทคโนโลยีหน่วยความจำในอนาคต เนื่องจากการประยุกต์ใช้งานได้อย่างมีประสิทธิภาพในหน่วยความจำประเภทเข้าถึงโดยสุ่มแบบความต้านทาน (resistive random access memory, RRAM) การทำความเข้าใจพฤติกรรมของการเปลี่ยนกลับค่าความต้านทานในอุปกรณ์ขนาดเล็กมีความสำคัญต่อการพัฒนา RRAM และการปรับขนาดของ RRAM นั้นจำเป็นต้องมีความเข้าใจอย่างละเอียดเกี่ยวกับกลไกการสลับสถานะ ในงานวิจัยฉบับนี้ เราศึกษาพฤติกรรมการเปลี่ยนกลับค่าความต้านทานในเส้นลวดนาโนซิงออกไซด์ด้วยกล้องจุลทรรศน์แรงอะตอมแบบการวัดความนำไฟฟ้า ซึ่งความสัมพันธ์ระหว่างกระแสไฟฟ้ากับศักย์ไฟฟ้าสามารถวัดได้โดยใช้เข็มของกล้องจุลทรรศน์แรงอะตอมที่ทำจากโลหะแพลทินัมทำหน้าที่เป็นขั้วไฟฟ้าด้านบนและใช้ฐานของเส้นลวดนาโนซิงออกไซด์ซึ่งเคลือบด้วยโลหะเงินทำหน้าที่เป็นขั้วไฟฟ้าด้านล่าง ผลการทดลองพบว่า การเปลี่ยนกลับค่าความต้านทานในเส้นลวดนาโนซิงออกไซด์เป็นได้ทั้งแบบที่ใช้ศักย์ไฟฟ้าขั้วเดียวและแบบสองขั้ว โดยพฤติกรรมการเปลี่ยนกลับค่าความต้านทานไม่ขึ้นอยู่กับขนาดของเส้นลวดนาโนซิงออกไซด์ ซึ่งบ่งบอกถึงการเปลี่ยนกลับค่าความต้านทานนั้นเกิดขึ้นได้เนื่องจากเส้นใยนำไฟฟ้า ทั้งนี้กราฟแสดงความสัมพันธ์ระหว่างกระแสไฟฟ้ากับศักย์ไฟฟ้าแสดงให้เห็นว่า สถานะที่มีความต้านทานต่ำมีการนำไฟฟ้าแบบผสมระหว่างการนำไฟฟ้าแบบโอห์มมิกหรือแบบ space-charge-limited current ส่วนสถานะที่มีความต้านทานสูงมีการนำไฟฟ้าแบบโอห์มมิกรวมกับแบบ space-charge limited current

สาขาวิชาฟิสิกส์
ปีการศึกษา 2561

ลายมือชื่อนักศึกษา อรรถิ ศรีกิมแก้ว
ลายมือชื่ออาจารย์ที่ปรึกษา Utsom Kunthakorn

ORADEE SRIKIMKAEW : STUDYING RESISTIVE SWITCHING
BEHAVIOR IN ZINC OXIDE NANOWIRES WITH ATOMIC FORCE
MICROSCOPE. THESIS ADVISOR : WORASOM KUNDHIKANJANA,
Ph.D. 48 PP.

NON-VOLATILE MEMORY/RESISTIVE SWITCHING/ZINC-OXIDE
NANOWIRES/CONDUCTIVE ATOMIC FORCE MICROSCOPE

Studying resistive switching (RS) phenomena is important for next-generation memory technology due to their potential applications in resistive random access memory (RRAM). Understanding RS behavior in small device sizes is important for the development of RRAM, and the scaling of RRAM requires a detailed understanding of switching mechanisms. In this work, we study resistive switching in ZnO nanowire using conductive atomic force microscopy (C-AFM). The $I-V$ characteristic measurement was performed on the Pt/ZnO nanowire/Ag devices. We found that ZnO nanowires exhibit both unipolar and bipolar switching behaviour. The RS behaviors are independent of the nanowires size, suggesting that the switching is due to conductive filaments. The conduction mechanisms demonstrating the low resistance state are mixed behaviors with either Ohmic conduction or space-charge-limited conduction. The high resistance state is dominated by Ohmic conduction followed by space-charge-limited conduction.


School of Physics

Academic Year 2018

Student's Signature



Advisor's Signature



ACKNOWLEDGEMENT

I wish to thank my advisor Dr. Worasom Kundhikanjana for her endless patience, support, guidance, and advice provided over the course of my thesis. I would also like to thank the thesis examining committee, including Dr. Nuanwan Sanguansak, Dr. Annop Klamcheun, and Assoc. Prof. Dr. Puangratana Pairor for their helpful and suggestions during my thesis defense. I would like to thank my family and my friends, Panithan Sriboriboon and Sartanee Suebka, for constant support throughout the learning process and encouragement.

I wish to thank Development and Promotion of Science and Technology Talents Project Scholarship Program, Thailand, and Center for Scientific and Technological Equipment (CSTE), Suranaree University of Technology (SUT). This project is supported by Thailand Research Fund (TRF) <http://www.trf.or.th/> (contract number TRG5880060), Suranaree University of Technology (SUT) www.sut.ac.th, and (contract number SUT1-105-59-12-11 and SUT1-105-58-12-22), NANOTEC-SUT Center of Excellence on Advanced Functional Nanomaterials, and the Office of the Higher Education Commission under the National Research University (NRU) project.

Oradee Srikimkaew

CONTENTS

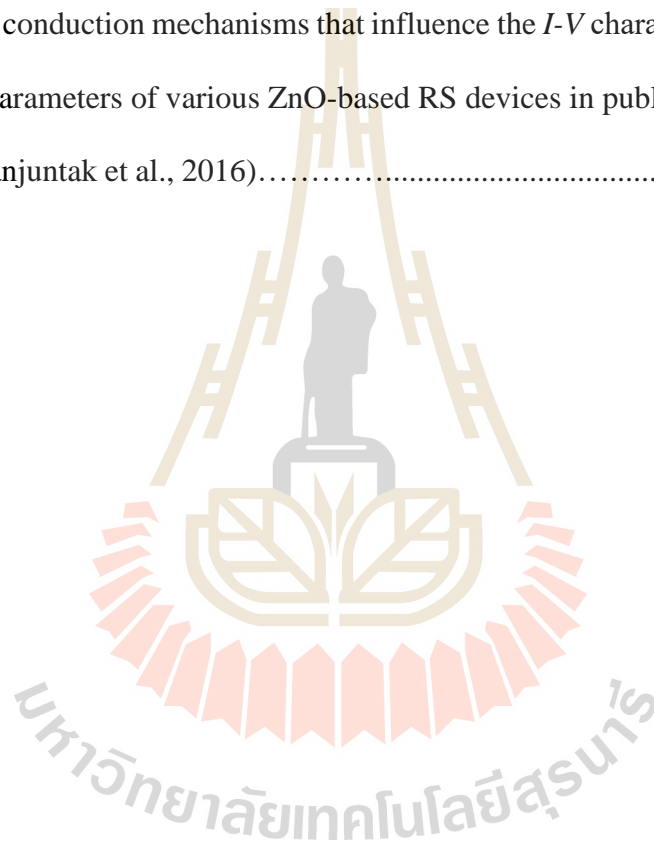
	Page
ABSTRACT IN THAI.....	I
ABSTRACT IN ENGLISH.....	II
ACKNOWLEDGEMENTS.....	III
CONTENTS	IV
LIST OF TABLES	VI
LIST OF FIGURES	VII
CHAPTER	
I INTRODUCTION	1
1.1 Resistive Random Access Memory.....	2
1.2 Resistive Switching Phenomena	3
1.3 Zinc Oxides.....	4
1.4 Atomic Force Microscope.....	6
1.5 Application of C-AFM for Resistive Switching Observations.....	7
1.6 Research Objectives	10
1.7 Thesis Outline	10
II REVIEW OF RESISTIVE SWITCHING PHENOMENA IN	
 MATERIAL OXIDES.....	12
2.1 Migration of Oxygen Vacancies.....	12
2.2 Unipolar Switching Mechanism.....	13

CONTENTS (Continued)

	Page
2.3 Bipolar Switching Mechanism.....	15
2.4 Current Conductions	18
2.5 Resistive Switching Investigations of ZnO Materials.....	20
III METHODS	25
3.1 ZnO Nanowires Growth.....	25
3.2 <i>I-V</i> Characteristic Measurements.....	26
3.3 Homemade LabVIEW Data Acquisition Program.....	27
IV RESULTS AND DISCUSSION.....	29
4.1 <i>I-V</i> Characteristics	29
4.2 Conduction Mechanisms.....	33
4.3 Size-independence <i>I-V</i> Characteristics.....	37
4.4 <i>I-V</i> Characteristics of Sm-substituted BFO.....	39
V CONCLUSIONS.....	41
REFERENCES	43
CURRICULUM VITAE.....	48

LIST OF TABLES

Table	Page
1.1 The properties of ZnOs.....	5
2.1 Basic conduction mechanisms that influence the <i>I-V</i> characteristic.....	19
2.2 The parameters of various ZnO-based RS devices in published literature (Simanjuntak et al., 2016).....	20



LIST OF FIGURES

Figure	Page
1.1	Typical device structure for RRAM applications.....2
1.2	Typical operation of RS. The forming, reset, and set processes occur in the dielectric material according to the V_{ext} that is applied. The flowing current is limited in term of a compliance current.....4
1.3	Typical I - V curves of unipolar and bipolar switching.....4
1.4	The wurtzite structure of ZnO unit cell.....5
1.5	Schematic of the AFM operation. The interaction between the tip and the sample causes the cantilever bend up and down. The change in the position of the laser beam will generate height information on the photodetector and is converted into images.....6
1.6	Schematic of the C-AFM operation. The current can by applying voltage between the tip and the electrode at the bottom of the sample. The flowing current, I is displayed as a function of bias voltage, V7
1.7	C-AFM measurements on TiO ₂ films (Chae et al., 2008)8
1.8	AFM topography images associated with current maps (a) and (c) in the HRS, (b) and (d) in the LRS (Zhuge et al., 2011)9
1.9	(a) AFM topography image was taken on a single ZnO nanoisland, and corresponding current maps (C-AFM image) of the LRS (b) and the HRS (c). Adapted from (Qi et al., 2013)9

LIST OF FIGURES (Continued)

Figure	Page
2.1	The behavior of conductive filaments in oxide materials during RS operations (Lee et al., 2015).....14
2.2	A virtual cathode model used to explain the polarity-dependent operation. Adapted from (Lee et al., 2015)16
2.3	A Schottky barrier of an n-type semiconductor: (a) band diagrams before joining; (b) band diagram of the junction at equilibrium.....17
2.4	The modulation of the Schottky barrier by oxygen vacancies migration. Adapted from (Lee et al., 2015)17
2.5	The modulation of the Schottky barrier by trapping and detrapping of electrons. Adapted from (Lee et al., 2015)18
2.6	The in situ TEM images of the filament formation (a) and rupture (b) processes in real time observed in a ZnO film. (c) The corresponding $I-V$ curve. Adapted from (Chen et al., 2013)21
2.7	(a) Bipolar switching behaviors of Cu/ZnO-NW/Pd memory devices. (b) EDX elemental mappings in LRS. (c) The corresponding SEM image. Adapted from (Yang et al., 2011)22
2.8	The relation of current density versus electric field ($J-E$) of the Pt/ZnO thin film/Pt device (Chang et al., 2008)24

LIST OF FIGURES (Continued)

Figure	Page
2.9	(a) The I - V curve of the Ag/ZnO microwire/Ag device. (b) The plots of $\ln I - \sqrt{V}$, $\ln(I/V) - \sqrt{V}$, and $I - V^2$ for the Schottky, PF, and SCLC conduction mechanisms, respectively (Huang et al., 2014)24
3.1	SEM image of the ZnO nanowire.....26
3.2	(a) Schematic of the C-AFM setup. (b) AFM topography image of the ZnO nanowires taken with 25Pt300A model cantilever.....28
3.3	A homemade LabVIEW program was used to control the input voltages And store data on input voltages, V and electrical current, I28
4.1	Typical I - V curve of single ZnO nanowire. The voltage was applied in the following sequence: 0 V to 10 V, 10 V to 0 V, 0 V to -10 V and -10 V to 0 V, at 0.025 V/s and compliance current of 0.1 mA. Both unipolar (a) and bipolar (b) behaviors were observed.....30
4.2	Typical unipolar RS behavior was observed by applying only positive voltage sweep with a compliance current 0.1 mA. The forming, reset and set processes are shown in black, red and blue curves.....31
4.3	Repeated switching observed on a single ZnO nanowire. (a) The I - V curve of 5 switching cycles, (b) reset and set voltages distribution as a function of cycle's number.....32
4.4	Box plot of $V_{FORMING}$, V_{RESET} , and V_{SET} taken from 20 nanowires. The crosses indicate the average value.....33

LIST OF FIGURES (Continued)

Figure	Page
4.5	LRS I - V characteristics. (a) Two switching cycles of a single ZnO nanowire, and (b) of different nanowires in LRS showing Ohmic and SCLC conduction.....35
4.6	HRS I - V characteristics of two nanowires show Ohmic conduction at low voltage and SCLC conduction at high voltage.....36
4.7	Typical I - V curve of bipolar RS behavior. The right (left) inset shows the positive (negative) voltage regime of the I - V curve in a log-log scale.....36
4.8	The resistance of unipolar RS behavior as a function of the nanowire cross-section area. (a) Distribution of Ohmic and SCLC behaviors and (b) on-off ratio for different nanowire cross-sections.....38
4.9	Box plot of $V_{FORMING}$, V_{RESET} , and V_{SET} taken from 20 nanowires. The crosses indicate the average value.....39
4.10	(a) Typical hysteresis loop in I - V curve of Sm 5%-BFO measured by C-AFM. (b) The forward I - V curves with Schottky model fitting (black curve) and (c) SCLC model fitting.....40

CHAPTER I

INTRODUCTION

Resistive switching (RS) phenomena have attracted great interest due to their potential applications in non-volatile memory known as resistive random access memory (RRAM). RS phenomena have been studied most widely in oxide materials. Among the oxide materials that exhibit RS phenomena, zinc oxide (ZnO) has several advantages, such as low cost and low synthesis temperature (Kasamechonchung et al., 2015). RS behavior in ZnO films are known to be occurred due to the formation of filament conductive paths; however, the RS behavior in ZnO nanowires may differ depending on surface areas and lengths.

In this thesis, we study RS behavior in ZnO nanowires using conductive atomic force microscopy (C-AFM). The ZnO nanowires were vertically growth on an Ag/glass substrate using a hydrothermal method, which serves as a bottom electrode. A C-AFM tip serves as a top electrode. By applying external voltage to the tip, *I-V* characteristics of individual nanowire were obtained.

In this chapter, we briefly describe the principle of RRAM and the characteristic, basic operation, and classification of RS phenomena. The properties and structure of ZnO nanowires will also be described. Next, we will introduce the C-AFM, which was used to study the RS behavior of ZnO nanowires. Lastly, we will discuss the research objectives and the thesis outline.

1.1 Resistive Random Access Memory

Memory can be subdivided into two main types: volatile and non-volatile. Volatile memory only maintains stored information while the device is powered, whereas non-volatile memory can maintain stored information even when the power is turned off. Resistive random access memory (RRAM) is a next generation non-volatile memory, which has a simpler, smaller, and faster operation time than other non-volatile memory (Chang et al., 2008; Waser and Aono, 2007). RRAM operations are based on RS phenomena where the resistance changes between two resistance states with the application of an external electric field. Figure 1.1 shows a schematic device structure for RRAM applications. The device structure consists of a dielectric material layer which is sandwiched between two metal electrodes: a top electrode (T.E.) and a bottom electrode (B.E.). When a voltage is applied to the electrodes, the resistance of the material can vary.

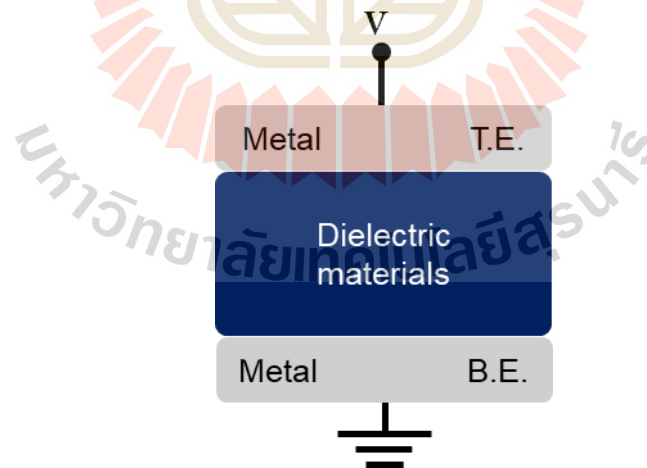


Figure 1.1 Typical device structure for RRAM applications.

1.2 Resistive Switching Phenomena

Resistive switching (RS) phenomena are a reversible change in resistance of materials between a high resistance state (HRS) and a low resistance state (LRS) when an external electric field is applied. The two resistance states of RS are stable for a long time after switching and can be used as binary states of RRAM.

Normally, the changes in resistance of RS phenomena are controlled by applying an external voltage, V_{ext} , and we can easily observe the behavior from the current-voltage (I - V) characteristic. Lee et al. (Lee et al., 2015) divided the typical behavior of RS into three main processes: forming, reset, and set as shown in Figure 1.2. The first process is “forming”, the resistance of dielectric materials changes from the pristine state to the LRS when enough V_{ext} is applied. The current thus flow throughout the device. By applying V_{ext} once more, the resistance remains in the LRS and switches to the HRS when the applied voltage reaches the reset voltage, V_{RESET} , called a “reset” processes. As the voltage is increased further and reaches the set voltage, V_{SET} , the resistance switches to the LRS again. Called a “set” process. During the reset and the set processes, the resistance switches between a high and a low value according to the V_{ext} that is applied. Owing to the higher current can cause the dielectric breakdown in a device, the flowing current in the forming and the set processes needs to be limited.

RS behavior can be classified into two types based on their responses to the V_{ext} : unipolar and bipolar switching. Figure 1.3 shows the I - V characteristics of unipolar and bipolar switching after the forming process. Unipolar switching requires only one polarity of V_{ext} (positive or negative) for switching between set and reset processes, whereas bipolar switching requires both two polarities.

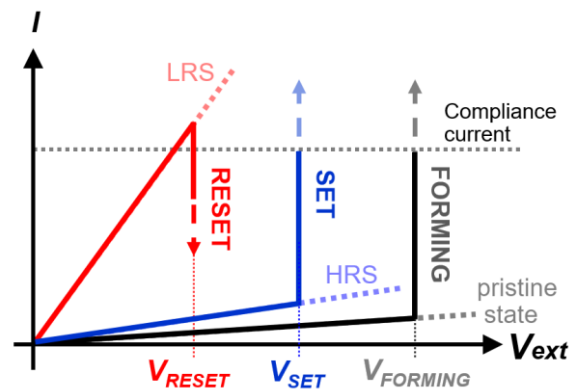


Figure 1.2 Typical operation of RS. The forming, reset, and set processes occur in the dielectric material according to the V_{ext} that is applied. The flowing current is limited in term of a compliance current.

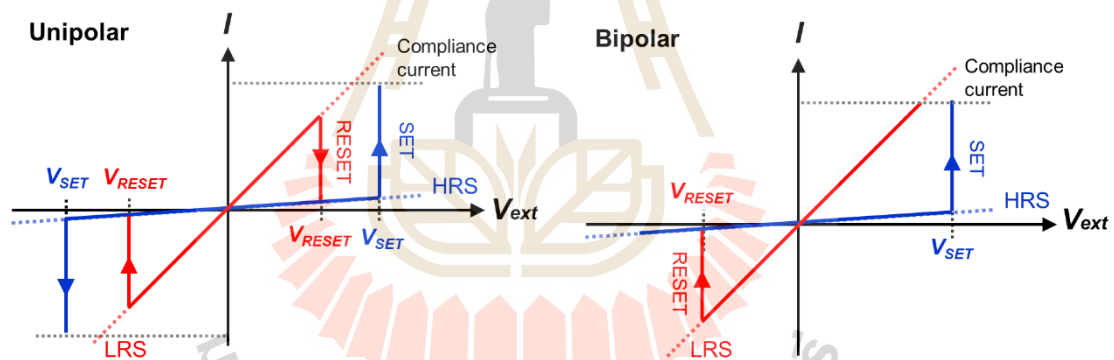


Figure 1.3 Typical I - V curves of unipolar and bipolar switching.

1.3 Zinc Oxides

Zinc oxide (ZnO) is among the most widely used materials of semiconductor devices. Owing to the wide range of properties as shown in Table 1.1 (Zhang, 1996), ZnO has been considered for application in light-emitting diodes (LED), lasers, sensors, and solar cells (Cui, 2012; Schmidt-Mende and MacManus-Driscoll, 2007). Undoped ZnO generally shows n-type semiconductor behavior due to existence of oxygen

vacancies. Its conductivity is in between 10^{-17} and $10^3 \Omega^{-1}\text{cm}^{-1}$ (Zhang, 1996), which can be tailored by doping or controlling native defects such as oxygen vacancies and zinc interstitials. Therefore, the change in chemical defects such as oxygen vacancies would change charge carrier concentrations, which are important for controlling the electrical properties of ZnO nanostructures.

Moreover, the crystalline structure of ZnOs is a hexagonal wurtzite structure as shown in Figure 1.4. One unit cell includes one Zn ion (red) surrounded by four O ions (blue), or vice versa.

Table 1.1 The properties of ZnOs.

Physical properties	Value
Lattice	Hexagonal. wurtzite
Lattice constants	$a = 0.324 \text{ nm}$, $c = 0.519 \text{ nm}$, $c/a = 1.60$
Band gap energy	3.2 eV
Dielectric constant	8.66
Refractive index	2.008
Specific heat	9.66 cal/(mol-K)
Intrinsic carrier concentration	$< 10^6 \text{ cm}^{-3}$
Mobility (300 K)	100-200 cm^2/Vs (electron), 5-50 cm^2/Vs (hole)
Melting point	2248 K

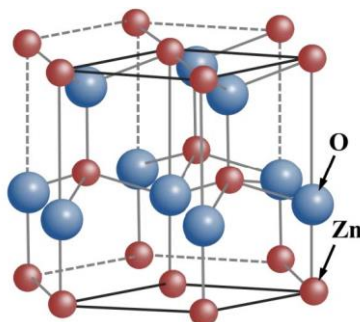


Figure 1.4 The wurtzite structure of ZnO unit cell.

1.4 Atomic Force Microscope

Atomic force microscopy (AFM) is a type of scanning probe microscopy, which is designed to measure local properties. AFM operates by using a sharp tip to scan over the sample surface, while the interaction between the end of the tip and the sample bends the cantilever up and down. The laser is focused on the cantilever, and the reflected signal from the backside of the cantilever is detected by the photodetector as shown in Figure 1.5. The signal from photodetector is converted into images.

Moreover, AFM is divided into three operating modes: contact, non-contact, and tapping. During the contact mode, the tip is always contacted to the sample surface, which can damage a soft sample. In the non-contact mode, the cantilever is set to oscillate at the resonance frequency. If the tip oscillates very close to the sample, the tip can contact with the sample periodically. This is referred to the tapping mode.

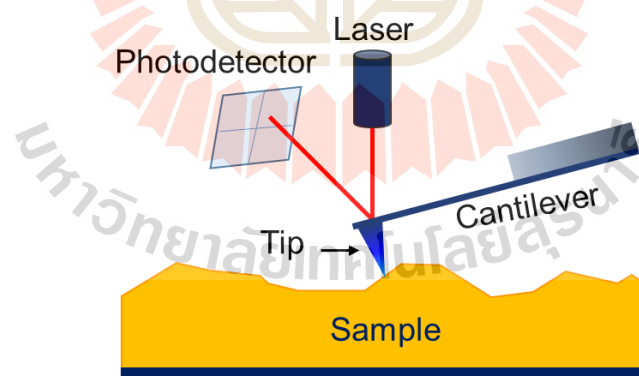


Figure 1.5 Schematic of the AFM operation. The interaction between the tip and the sample causes the cantilever bend up and down. The change in the position of the laser beam will generate height information on the photodetector and is converted into images.

In order to verify the resistance of the sample, conductive atomic force microscopy (C-AFM) is techniques employed for I - V measurements. C-AFM is based on the contact mode, and use a conductive cantilever acts as an electrode. Figure 1.6 shows a schematic of the CAFM operation. A bias voltage is applied between a conductive tip and an electrode at the bottom of the sample leading to a flow of current in the sample. The I - V characteristic of the sample is obtained.

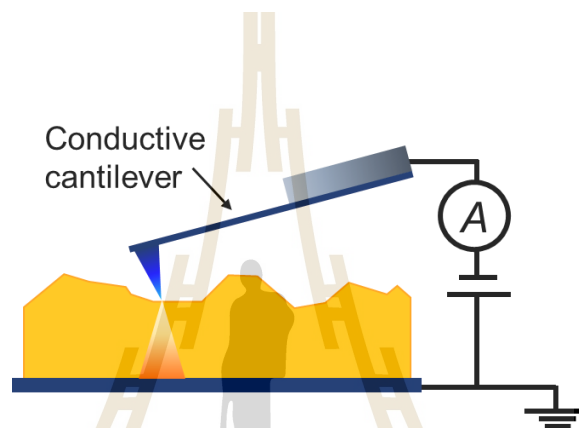


Figure 1.6 Schematic of the C-AFM operation. The current can occur by applying voltage between the tip and the electrode at the bottom of the sample. The flowing current, I is displayed as a function of bias voltage, V .

1.5 Application of C-AFM for Resistive Switching Observations

In an attempt to study the microscopic mechanism of RS phenomena, CAFM has been demonstrated to be a powerful technique for studying RS at the nanoscale (Lanza, 2014). Chae et al. are one of the most researchers that used C-AFM to describe how the conductive path takes place during RS operations (Chae et al., 2008). Figure 1.7 shows the C-AFM measurements on TiO₂ films, while Figure 1.7(a) is the schematic diagram of the measurements, which TiO₂ film sandwiched between AFM tip (T.E.) and Pt (B.E.). Figure 1.7(b) is the obtained I - V characteristics, which exhibits the unipolar

switching. Figure 1.7(c) and (d) show current maps of the film surface for LRS (after forming) and HRS (after reset), respectively. The local conducting regions were observed in LRS, but not in HRS. The result shows that the conductive paths appear in LRS, and disappear when the sample is in HRS, which consistent with formation and rupture of conductive filaments.

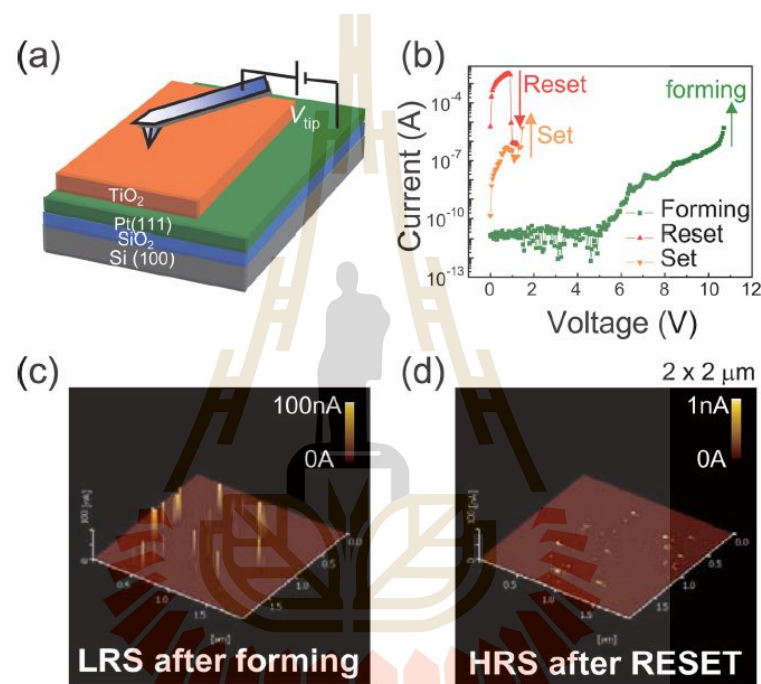


Figure 1.7 C-AFM measurements on TiO₂ films (Chae et al., 2008).

For RS in ZnOs, C-AFM was also used to confirm the formation of conductive filaments in the grain boundaries of ZnO film (Zhuge et al., 2011). Figure 1.8 shows the AFM topography images associated with the current maps, while Figure 1.8(a) and (c) are images when the film was in HRS (OFF state), and Figure 1.8(b) and (d), the film was in LRS (ON state). This result shows that the conductive paths were formed in LRS which located at the grain boundaries suggested by comparing Figure 1.8(b) and (d). In other experiment, Figure 1.9 shows the topography image and current

maps of ZnO nanoislands taken by AFM (Qi et al., 2013). Unlike a small conductive filament in ZnO films, the current tends to distributed around the edge of nanoislands. This result indicates that the conductive pathway in ZnO nanostructure maybe different from ZnO films.

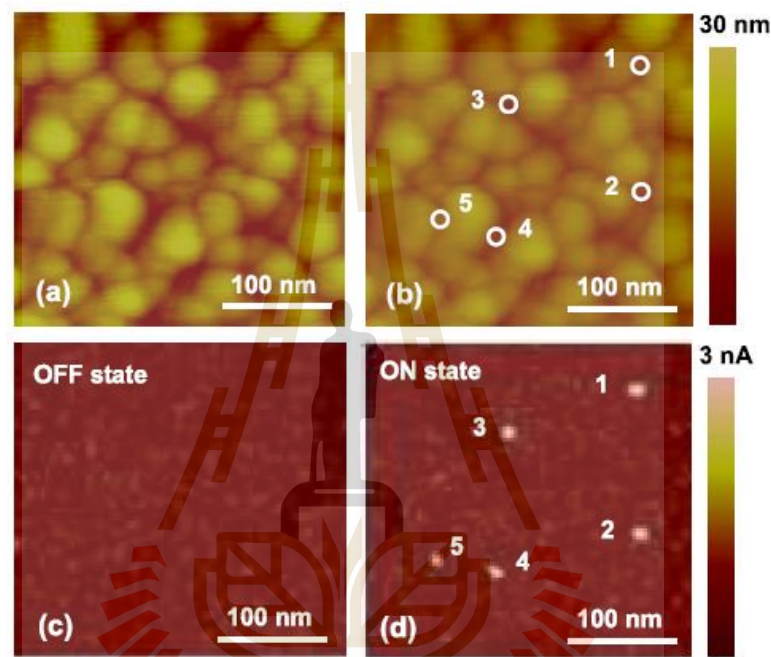


Figure 1.8 AFM topography images associated with current maps (a) and (c) in the HRS, (b) and (d) in the LRS (Zhuge et al., 2011).

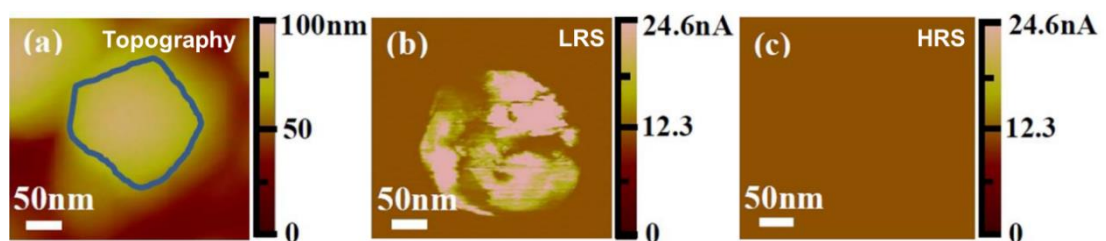


Figure 1.9 (a) AFM topography image was taken on a single ZnO nanoisland, and corresponding current maps (C-AFM image) of the LRS (b) and the HRS (c). Adapted from (Qi et al., 2013).

1.6 Research Objectives

In this work, we aim to investigate the RS behavior of the n-type ZnO nanowires using C-AFM. We assemble a metal—ZnO nanowires—metal structure experimental device, and measure the *I-V* characteristic of individual ZnO nanowire by applying an external voltage to the AFM cantilever. By using C-AFM, the variation of nanowire sizes also be observed. We hope to know the switching types and understand the conduction mechanism of the RS behavior in ZnO nanowires. Eventually, better understanding of RS mechanism will be used for development of RRAM devices.

1.7 Thesis Outline

This thesis is divided into five chapters. Chapter I gives a brief overview of the rationale of this research. We introduce the significance of RS phenomena and the advantages of studying ZnO nanowires using C-AFM.

Chapter II explains the RS phenomena that occurs in oxide materials. Mechanisms of unipolar switching and bipolar switching behaviors are described, which focuses on the role of oxygen vacancies and electrons. The polarity-dependence of bipolar switching is discussed in three possible models: virtual cathode, oxygen vacancies migration, and electrons trapping. The conduction mechanisms that influence the *I-V* characteristics also be described. The last section review the investigations of RS in ZnO materials.

In chapter III, we explain our methodology consisting of ZnO nanowires growth and the procedures of RS investigation. We perform the *I-V* characteristic measurements, where the ZnO nanowire sample is sandwiched between the AFM tip and the sample substrate.

Our results are described in chapter IV. This chapter is divided into three sections: *I-V* characteristics, conduction mechanisms and size-independence *I-V* characteristics. We propose both unipolar and bipolar behavior and mixed conduction mechanisms observed in ZnO nanowires.

In chapter V, we present the conclusion of this work, and suggestion for future work.



CHAPTER II

REVIEW OF RESISTIVE SWITCHING PHENOMENA IN MATERIAL OXIDES

RS phenomena have been studied most widely in oxide materials due to its common defects that are oxygen vacancies. The concentration and migration of oxygen vacancies has an effect on oxides properties, especially the electrical resistance. The migration of oxygen vacancies plays a vital role in the changes of resistance which lead to RS phenomena. Therefore, understanding the role of oxygen vacancies in RS phenomena is important.

This chapter begins by giving a brief overview of the migration of oxygen vacancies in oxide materials. In the section 2.2 and 2.3, we will discuss the switching mechanisms of unipolar and bipolar switching. The current conduction mechanisms that influence the I - V characteristics also be described in the section 2.4. The final section reviews the RS investigations of ZnO materials.

2.1 Migration of Oxygen Vacancies

The role of oxygen vacancies in RS devices has been described by Lee et al. (Lee et al., 2015). Oxygen vacancies can affect the resistance of oxides in one of three ways: (1) Oxygen vacancies can form in the conductive filaments when an electric field is applied. The formation and rupture of conductive filaments have an effect on the

changes of resistance between LRS and HRS. The behavior of conductive filaments is explained in section 2.2. (2) Oxygen vacancies can affect the height and width of Schottky barriers, which lead to changes of resistance. (3) Oxygen vacancies can form trap sites for electrons, the Schottky barrier can be modulated by the trapping and detrapping processes. Modulation of the Schottky Barrier is explained in section 2.3.

The migration of oxygen vacancies can be explained by one of three forces: electric field, Soret force, and Fick force. (1) In an electric field, oxygen vacancies (positive charge) will move toward the cathode. Oxygen ions (negative charge) will move toward the anode. (2) Without an electric field, a temperature gradient, ∇T (in terms of a Soret force) due to Joule heating can cause ionic motion. Oxygen ions will move from hotter regions to cooler regions because the velocity in hotter regions is higher than that in cooler regions; oxygen vacancies move conversely. (3) The migration can be achieved due to non-uniform distribution of the oxygen vacancies. Thus, to minimize the free energy, the oxygen vacancies should move from higher concentration regions to lower concentration regions. This case can be described in terms of the Fick force. These three cases for the migration of oxygen vacancies may be present simultaneously.

2.2 Unipolar Switching Mechanism

Many microscopic studies have proposed that unipolar switching in oxides is due to the formation and the rupture of conductive filaments (Lee 2015, Waser 2007, Sawa 2008). Figure 2.1 shows the behavior of conductive filaments during RS operations. A pristine oxide cell does not have conductive filaments as shown in Figure 2.1(a). When an electric field is applied, conductive filaments are formed and the cell

enters the LRS—the forming process (Figure 2.1(b)). The partial rupture of conductive filaments will occur when enough electric field is applied in the reset process and the cell enters the HRS (Figure 2.1(c)). The ruptured conductive filament is reconnected in the set process and the cell goes in to the LRS again. The formation and rupture of conductive filaments are induced by migration and percolation of defects (such as oxygen vacancies) or metallic ions, which assisted by an electric field and a thermal effect (Kim et al., 2011; Lee et al., 2015).

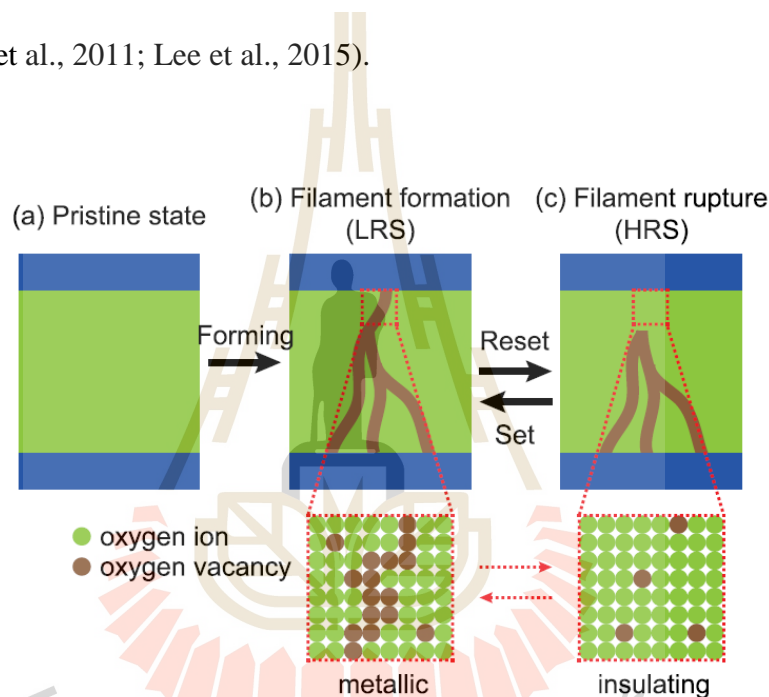


Figure 2.1 The behavior of conductive filaments in oxide materials during RS operations (Lee et al., 2015).

Moreover, the forming process has been described in terms of a soft dielectric breakdown phenomenon (Lee et al., 2015). Current flow inside the oxide cell is enabled by the formation of conductive filaments. Dielectric breakdown can be prevented by limiting the maximum electric current. The formation of conductive filaments depends on two forces for oxygen vacancies migration: the electric field and the Soret force. For

the reset process, the Fick force is dominant. The oxygen vacancies try to move from the conductive filaments (higher concentration) to the surrounding (lower concentration), thus the filament is ruptured. After the conductive filaments have ruptured, the electric current cannot flow throughout the oxide cell and the current drops suddenly.

2.3 Bipolar Switching Mechanism

Like unipolar switching, the conductive filaments can form between the top and bottom electrodes via the forming process. Thus the forming process is required for most bipolar switching.

After the forming process, the oxygen vacancies and electrons act as the majority carriers in electronic transport for bipolar switching, whose polarity-dependent operation is caused by the dominant carrier. Lee et al. (Lee et al., 2015). reported that the polarity-dependent operation can be explained by three models. The first two models are explained in terms of oxygen vacancies migration, and the last model is explained by trapping and detrapping of electrons.

2.3.1 Formation of Virtual Cathode

The accumulation of oxygen vacancies can produce a virtual cathode, which is a region with high concentration of oxygen vacancies, and has a higher conductance than the surrounding. Figure 2.2 shows the behavior of the virtual cathode in bipolar switching. Once the virtual cathode has formed, the gap region between the virtual cathode and the anode becomes small. When a negative voltage is applied to the anode, the virtual cathode is attracted to the anode, the oxygen vacancies percolate throughout the cell, and the sample enters the LRS. When a positive voltage is applied

to the anode, the virtual cathode is repelled from the anode, and the sample enter the HRS. Therefore, the set and reset processes occur at different polarities.

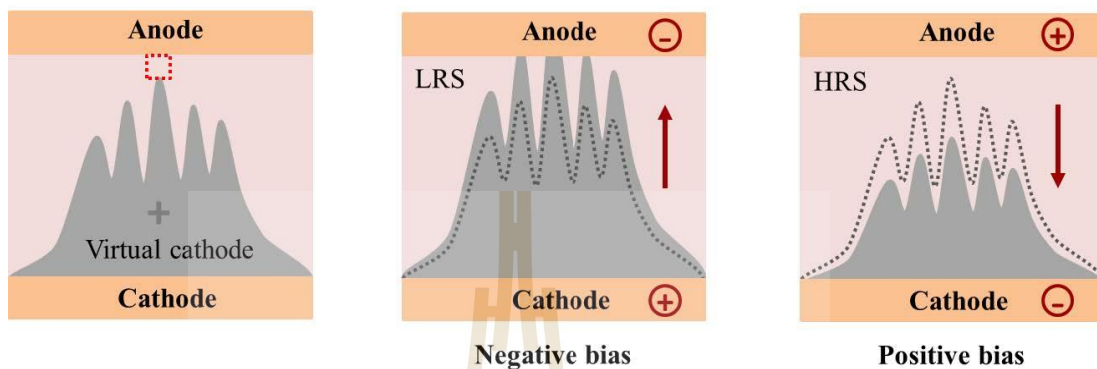


Figure 2.2 A virtual cathode model used to explain the polarity-dependent operation. Adapted from (Lee et al., 2015).

2.3.2 Modulation of the Schottky Barrier by Oxygen Vacancies Migration

The Schottky barrier can be formed in the metal—semiconductor (oxides layer)—metal junction, which depends on the work functions between the metal and semiconductor. For n-type semiconductors, the Schottky barrier can be formed when the work function of the metal is larger than that of the semiconductor as shown in Figure 2.3. Figure 2.3(a) shows the band diagrams of the metal and the semiconductor before joining. Figure 2.3(b) shows the band diagram of the junction at equilibrium. On the other hand, if the work function of metal is smaller than that of the semiconductor, the junction is an Ohmic contact. The width of the Schottky barrier is associated with the concentration of oxygen vacancies, their migration will affect the barrier width. Figure 2.4 shows the modulation of the Schottky barrier due to oxygen vacancies migration. When a negative voltage is applied to the anode, oxygen vacancies will

migrate toward the anode. Thus, the width of the Schottky barrier is narrowed and the cell enters the LRS, as shown in Figure 2.4(a). When a positive voltage is applied to the anode, oxygen vacancies will migrate from the anode, the width of the Schottky barrier is recovered and the cell enters the HRS, as shown in Figure 2.4(b).

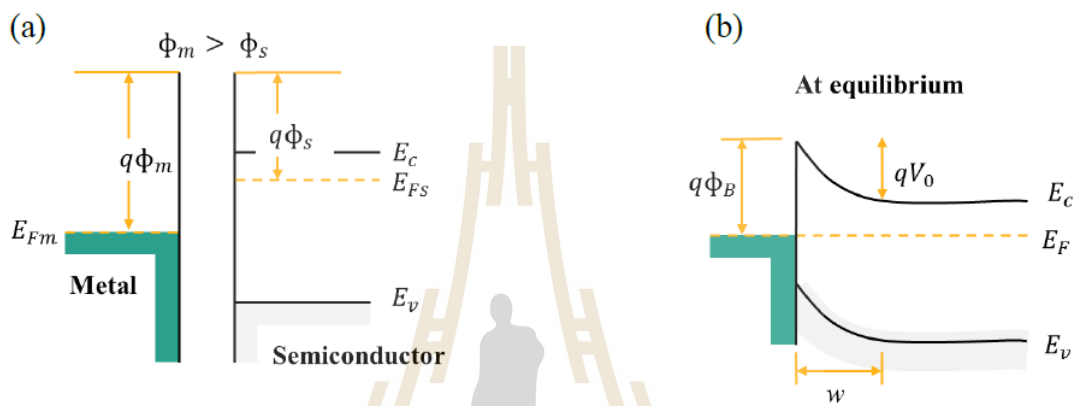


Figure 2.3 A Schottky barrier of an n-type semiconductor: (a) band diagrams before joining; (b) band diagram of the junction at equilibrium.

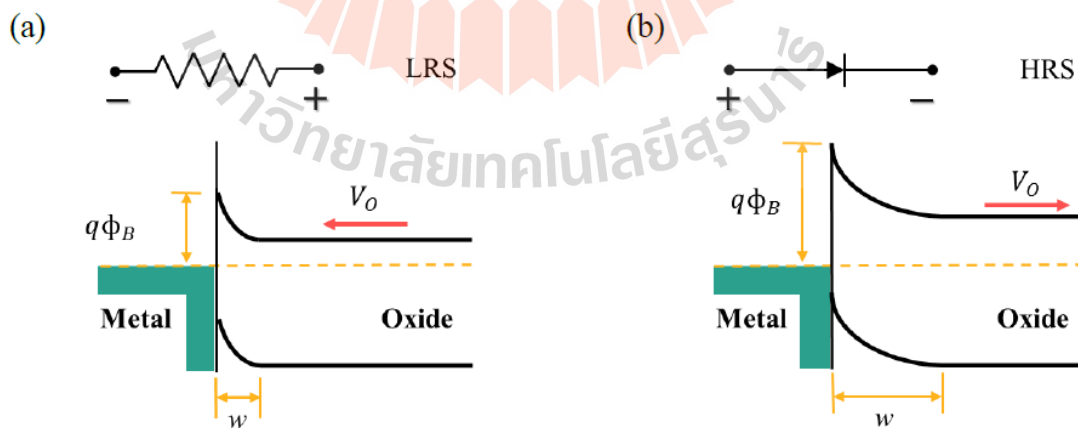


Figure 2.4 The modulation of the Schottky barrier by oxygen vacancies migration.

Adapted from (Lee et al., 2015).

2.3.3 Modulation of the Schottky Barrier by Electrons Trapping

In contrast to oxygen vacancies migration, the modulation of the Schottky barrier can be caused by trapped and detrapped electrons in oxides as shown in Figure 2.5. A negative voltage applied to the anode is similar to electrons injected into the oxide cell. These electrons are trapped in defects, thus widening the width of the Schottky barrier. For this reason, the tunneling current decreases and the cell enters the HRS. On the other hand, when a positive voltage is applied to the anode, the electrons are detrapped. The barrier is narrowed and the cell enters the LRS.

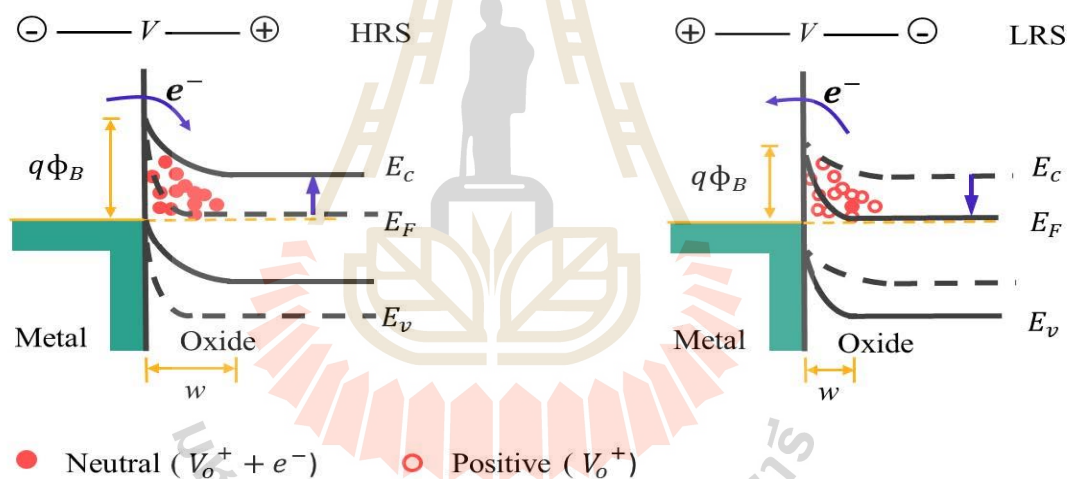


Figure 2.5 The modulation of the Schottky barrier by trapping and detrapping of electrons. Adapted from (Lee et al., 2015).

2.4 Current Conductions

The study of conduction mechanisms is important for understanding RS due to the current conduction associate the change in resistance of materials during applying voltages. Current conduction in semiconductors has many different mechanisms and

very complicated. Table 2.1 shows the basic conduction mechanisms that influence the I - V characteristics of metal-semiconductor contacts (Sze and Ng, 2006). These five mechanisms are (1) tunneling of electrons through the barrier at the contacts (dominant at high applied voltage and responsible for most Ohmic contacts), (2) Ohmic behavior is the common conduction which dominate under low voltage and high temperature, (3) space-charge-limited current (SCLC) is induced by carrier injection from the metal electrode and the charge is not compensated, (4) Schottky emission is thermionic emission of electrons over the Schottky barrier at metal-semiconductor contacts (responsible for Schottky contacts), (5) Poole-Frenkel emission is similar to Schottky emission, but the electrons are emitted from trapped sites into the conduction band and the barrier is lower than Schottky barrier.

Table 2.1 Basic conduction mechanisms that influence the I - V characteristics.

Conduction processes	Voltage & temperature dependence
Tunneling	$J \propto V^2 \exp\left(\frac{-b}{V}\right)$
Ohmic behavior	$J \propto V \exp\left(\frac{-c}{T}\right)$
Space-Charge-Limited Current	$J = \frac{9\varepsilon_i \mu V^2}{8d^3}$
Schottky emission	$J \propto T^2 \exp\left[\frac{q}{kT}(a\sqrt{V} - \phi_B)\right]$
Poole-Frenkel emission	$J \propto V \exp\left[\frac{q}{kT}(2a\sqrt{V} - \phi_B)\right]$

ϕ_B = barrier height. a , b , and c are constant. d = semiconductor thickness.
 ε_i = permittivity. μ = mobility.

2.5 Resistive Switching Investigations of ZnO Materials

RS of ZnO has been widely observed in various structures. The parameters of ZnO-based RS devices are shown in Table 2.2 (Simanjuntak et al., 2016). RS behaviors of ZnO can exhibit both unipolar and bipolar switching. All unipolar switching require the forming process, and the $V_{FORMING}$ is typically higher than the V_{RESET} and V_{SET} . Unlike unipolar switching, bipolar switching does not seem to require the forming process. Most devices are forming free — the resistance of the pristine state and the HRS are not distinct.

Table 2.2 The parameters of various ZnO-based RS devices in published literature (Simanjuntak et al., 2016).

Structure	Compliance current (mA)	$V_{FORMING}$ (V)	V_{RESET} (V)	V_{SET} (V)	Type
Pt/ZnO/Pt	30	~3.3	-1	~-2	U
Pt/ZnO/Pt	3	~4	~-0.5	~-1.2	B
Pt/ZnO/Pt	10	~4	~-0.5	~-1.5	U
Pt/ZnO/Ru	10	~4	~-0.7	~-1.9	U
Ru/ZnO/Pt	10	~4	~-1	~-2.1	U
TiN/ZnO/Pt	5	FF	-1.2	~-1.2	B
Au/ZnO/ITO	SC	FF	~-2	~-2	B
Al/ZnO/Al	1	NS	~-0.5	~-2.5	U
Al/ZnO/P ⁺⁺ -Si	5	1.56	2.07	~-1.41	U
TiN/ZnO/TiN	~80	FF	3	-4	B
Ag/ZnO/Pt	10	FF	~-0.4	0.8	B
Ag/ZnO/Cu	NS	2.5	~-1.3	~-1.3	B
Cu/ZnO/ITO	NA	4.42	0.6	2.6	U
Ag/a-ZnO/Pt	0.5	FF	-2	<0.5	B

SC self-compliance, FF forming free, U unipolar, B bipolar, NA data not available, NS not specified

2.5.1 Switching Mechanisms

The switching mechanism of ZnO-based RS devices has been described by the conductive filaments model. Chen et al. (Chen et al., 2013) observed the filament formation inside the ZnO film using *in situ* TEM as shown in Figure 2.6. They described the filament formation in term of the migration of oxygen ions, which leave the zinc ions and lead to form zinc metallic filaments. This region was identified as Zn-dominated ZnO_{1-x} metallic phase. When the oxygen ions migrate to metallic phase region, Zn-dominated ZnO_{1-x} phase transforms to ZnO phase—the zinc metallic filaments are ruptured. Like the zinc filament inside the films, the Cu filament was observed along the surface of ZnO nanowire by Yang et al. (Yang et al., 2011), as shown in Figure 2.7.

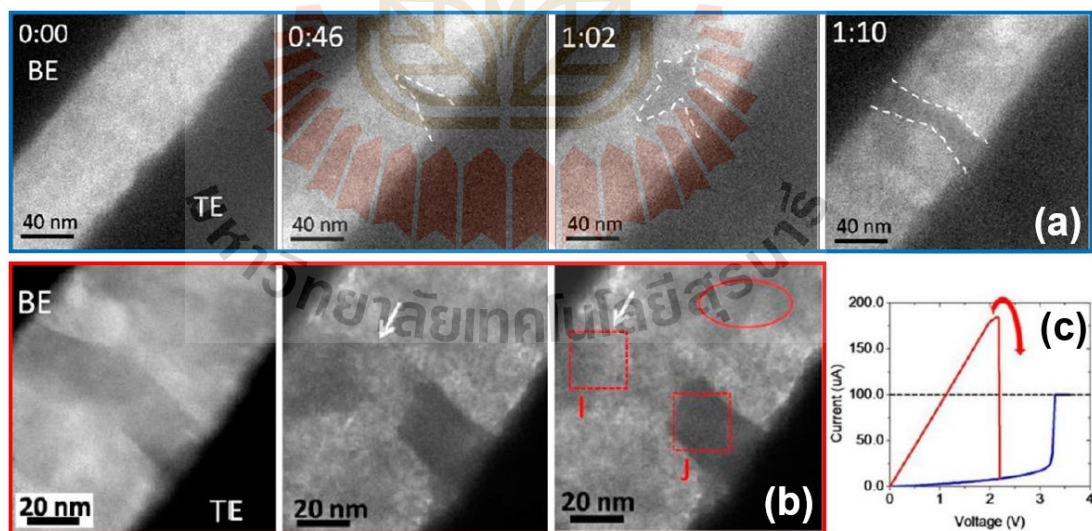


Figure 2.6 The *in situ* TEM images of the filament formation (a) and rupture (b) processes in real time observed in a ZnO film. (c) The corresponding $I-V$ curve. Adapted from (Chen et al., 2013).

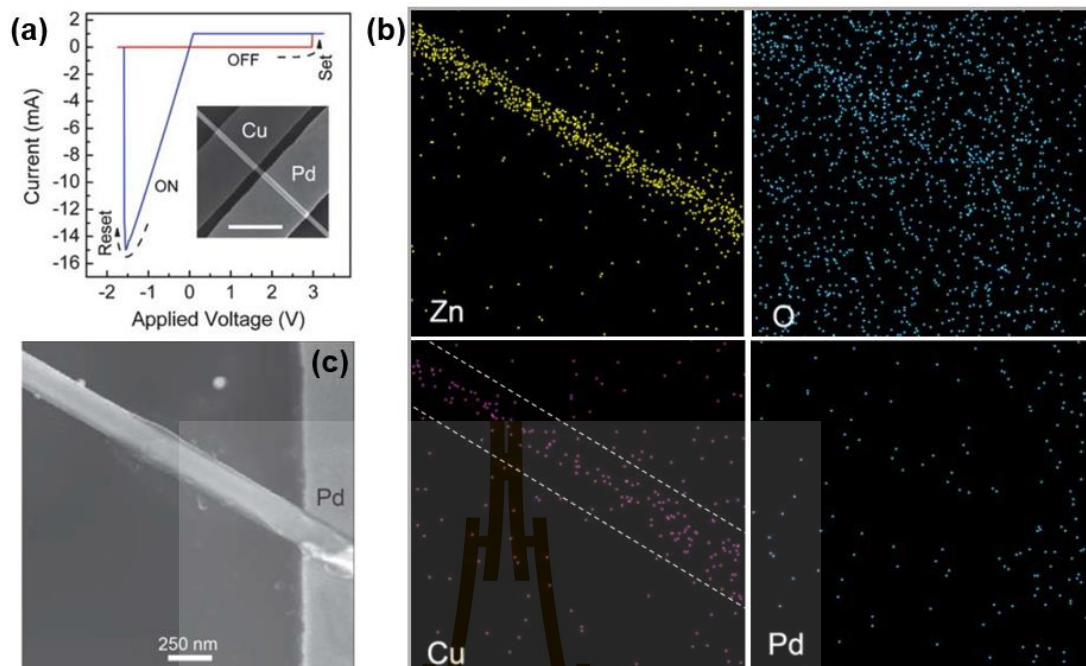


Figure 2.7 (a) Bipolar switching behaviors of Cu/ZnO-NW/Pd memory devices. (b) EDX elemental mappings in LRS. (c) The corresponding SEM image. Adapted from (Yang et al., 2011).

However, the switching mechanism of ZnO nanowires was described in term of surface diffusion of the metal adatoms (Raffone, Risplendi, and Cicero, 2016). Raffone et al. analyzed the results of Yang et al. via Density Functional Theory (DFT) calculations and proposed that the switching mechanism in ZnO nanowires was induced by doping effects of Cu adatoms rather than the filament formation. Because the nanowire length is the order of microns, which its device is thicker than the device-based thin film, under applied electric fields, Cu adatoms move on the surface easier than arrange together into the filaments. Cu adatoms are likely to spread out on the surface, lead to dope the insulating oxide and form the percolation path for the electrons.

The switching mechanism that causes the unipolar switching is clear for ZnO thin film. For ZnO nanowires, most studies have only tended to focus the bipolar switching, the unipolar switching mechanism is more complicated and unclear. The possible mechanisms are the formation of conductive filaments and the doping effect of metal electrodes suggested by the previous works of literature. As described, the switching mechanism of ZnO nanowire is still not widely understood.

2.5.1 Conduction Mechanisms

Unipolar RS behaviors of ZnO have also been described in terms of the current conduction. In ZnO films, the Ohmic conduction and the Poole-Frenkel emission dominated in the LRS and the HRS, respectively (Chang et al., 2008). The current density-electric field (J - E) relationships are shown in Figure 2.8. At low electric field region, the slope of both the LRS and HRS are close to 1, which indicate the Ohmic conduction. At high electric field region, the LRS still obeys the Ohmic conduction, whereas the HRS becomes Poole-Frenkel emission by curve fitting (inset Figure 2.8). Moreover, the LRS of ZnO microwires was also explained by Ohmic conduction (Huang et al., 2014). The I - V characteristic are shown in Figure 2.9. Unlike the HRS in ZnO films, the space-charge-limited conduction (SCLC) dominated in the HRS of ZnO microwires.

The conduction mechanisms of ZnO-based RS devices have been widely reported, however there are explained in many different ways. For the ZnO nanowires, the conduction mechanisms of unipolar switching have not been proposed, and it may be one of five conduction mechanisms as were described in section 2.4.

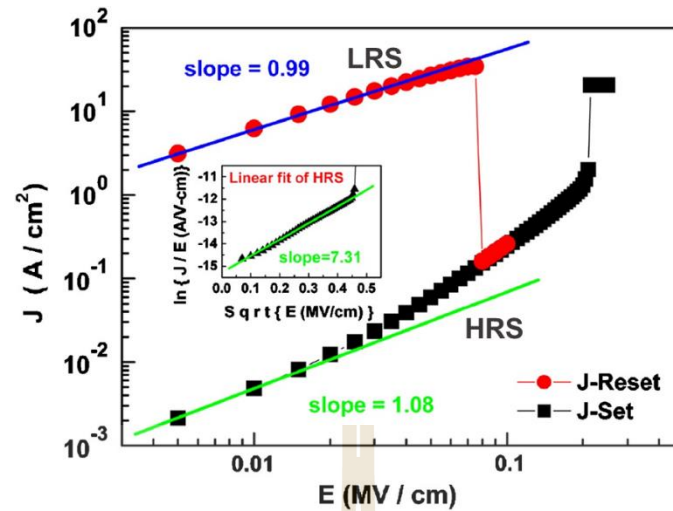


Figure 2.8 The relation of current density versus electric field (J - E) of the Pt/ZnO thin film/Pt device (Chang et al., 2008).

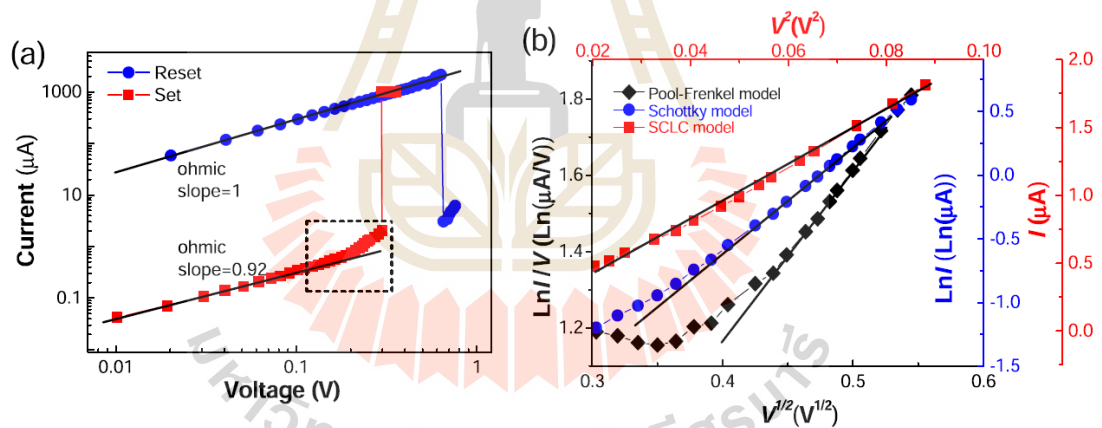


Figure 2.9 (a) The I - V curve of the Ag/ZnO microwire/Ag device. (b) The plots of $\ln I/\sqrt{V}$, $\ln(I/V) - \sqrt{V}$, and $I-V^2$ for the Schottky, PF, and SCLC conduction mechanisms, respectively (Huang et al., 2014).

CHAPTER III

METHODS

In chapter I, we described the device structure for RRAM applications Figure 1.1 which also applies for RS measurements. The device structure is similar to that of a capacitor, with two-terminal electrodes. In this chapter, we will explain three major components of this work: the ZnO nanowires growth, *I-V* characteristic measurement, and associated program.

To identify the structure of the nanowires, we take images of ZnO nanowires by using scanning electron microscopy (SEM). Second, we perform *I-V* characteristic measurements on the ZnO nanowires by using the substrate and the AFM tip as the electrodes. Then, we apply an external voltage to verify the resistance state of ZnO nanowires and measure the current that flows through the device via C-AFM.

3.1 ZnO Nanowires Growth

We acquired the ZnO nanowires samples from NANOTEC in collaboration with Dr. Annop Klamcheun. Figure 3.1 shows the SEM image of the ZnO nanowires were grown vertically on a Ag/glass substrate using a seed-assisted hydrothermal process as described in ref (Kasamechonchung et al., 2015). The seeded substrate was immersed in the 40 mM $(\text{Zn}(\text{NO}_3)_2 \cdot 6\text{H}_2\text{O})$ growth solution for 6 hours, which give about 1- μm -tall nanowires. The cross-section of the nanowires has a hexagonal shape. An average cross-section area of the nanowire is about $0.18 \mu\text{m}^2$. The Ag substrate forms

an Ohmic contact with the nanowires. The Ag substrate and the AFM probe serve as a bottom and top electrode for I - V characteristic measurements.

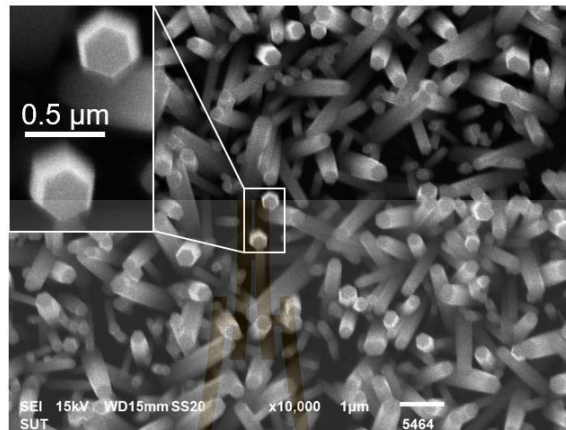


Figure 3.1 SEM image of the ZnO nanowire.

3.2 I - V Characteristic Measurements

The measurements were carried out on a XE-120 Park AFM, Park Systems Corp, Korea. Figure 3.2(a) shows schematic of our setup. The voltage was applied from the tip, while the sample was ground. The I - V characteristic measurement was carried out using Keysight B2900 source/measure unit. To ensure good electrical connection, we used solid platinum AFM probes (spring constant 18 N/m and resonance frequency 20 kHz 25PT300A, Rocky Mountain Nanotechnology, Salt Lake City, UT). The measurement procedure is the following:

- 3.2.1 Perform a $3\ \mu\text{m} \times 3\ \mu\text{m}$ topography image of a randomly selected region of the sample using a tapping mode AFM. Figure 3.2(b) shows an example topography image of the nanowires. The topography image was used as a

reference for landing on top of each nanowire for I - V characteristic measurements.

3.2.2 Choose a single nanowire to measure the current, I . The AFM tip was connected to this sample.

3.2.3 Switch to the C-AFM mode and apply a voltage from Keysight B2900 to the AFM tip and measure the current flowing from the AFM tip through the sample. During the measurement, the LabVIEW program will be used to control the input voltages and store data on input voltages, V and electrical current, I .

3.2.4 Repeat the measurement on other regions, the total of 20 NWs were measured from multiple AFM images.

The curve-fitting was done using Origin software (Microcal Software, Northampton, MA), and the nanowire cross-section areas were measured using ImageJ software.

3.3 Homemade LabVIEW Data Acquisition Program

The voltage sweep and data acquisition were performed using a homemade LabVIEW program. Figure 3.3 show our LabVIEW program function:

- 1) Connect with Keysight B2900 source/measure unit.
- 2) Specify the folder to store I - V data.
- 3) Define the CC, and I_T (threshold current, I_T is current value that use to stop apply voltage).

- 4) Define the number of points, the number of cycles and the voltage range.
- 5) Start the program with the “Sweep” button.

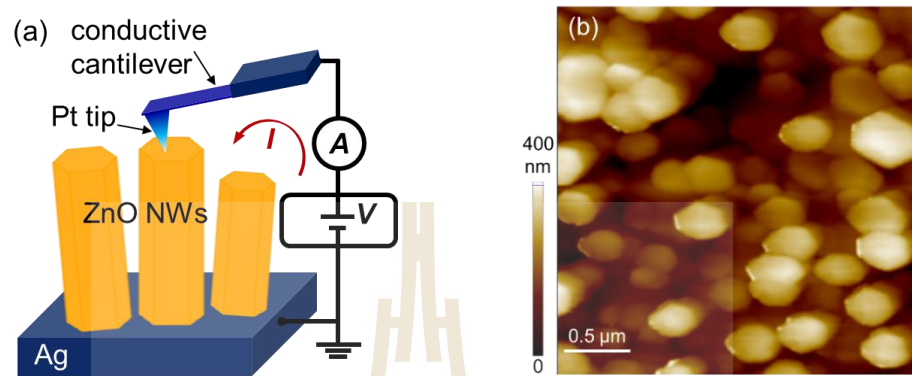


Figure 3.2 (a) Schematic of the C-AFM setup. (b) AFM topography image of the ZnO nanowires taken with 25Pt300A model cantilever.

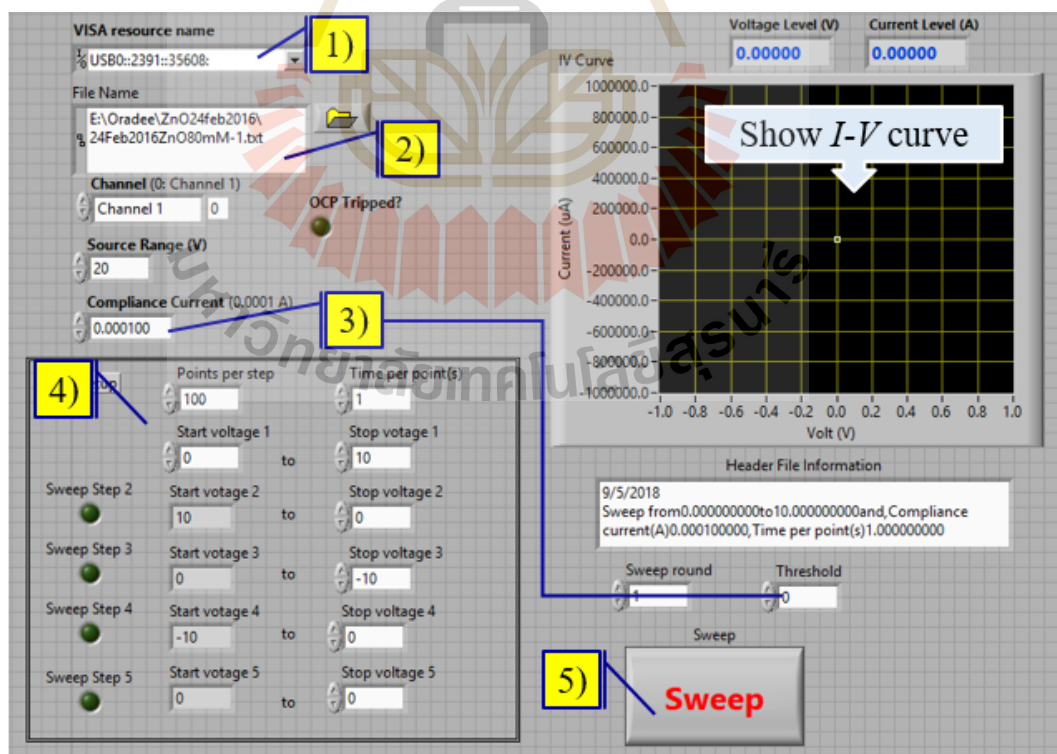


Figure 3.3 A homemade LabVIEW program was used to control the input voltages and store data on input voltages, V and electrical current, I .

CHAPTER IV

RESULTS AND DISCUSSION

The RS behavior can be observed in ZnO nanowires via C-AFM. In this chapter, we will discuss the results of this research study. Section 4.1 shows the I - V characteristics of the Pt/ZnO nanowire/Ag device. The I - V curves exhibited both the unipolar and bipolar switching types. The switching reproducibility will also be described. Section 4.2 demonstrates distributions of the switching voltage and the size-independence. Lastly, section 4.3 discusses the conduction mechanisms of RS in ZnO nanowires. The I - V characteristics are replotted in log-log scale with linear fitting.

4.1 I - V Characteristics

This section presents the typical I - V characteristics of ZnO nanowires that were observed by C-AFM with a Pt tip. Figure 4.1 shows the typical I - V characteristics of a single ZnO nanowire by applying voltage in the following sequence: 0 V to 10 V, 10 V to 0 V, 0 V to -10 V and -10 V to 0 V, at 0.025 V/s. The compliance current of 0.1 mA was used to prevent the permanent breakdown of the device. The current does not trace the same path in the forward and reward sweeps. During voltage sweeping, the resistance can change from the HRS to LRS (set process) and can switch back from the LRS to HRS (reset process). Figure 4.1(a) shows that the switching between the set and reset processes occurred in either positive or negative voltage sweep, which this I - V characteristic suggests the unipolar RS behavior, as was described in section 1.2.

Otherwise, the set and reset processes occurred in positive and negative voltage, respectively. This is the bipolar RS behaviour, as shown in Figure 4.1(b).

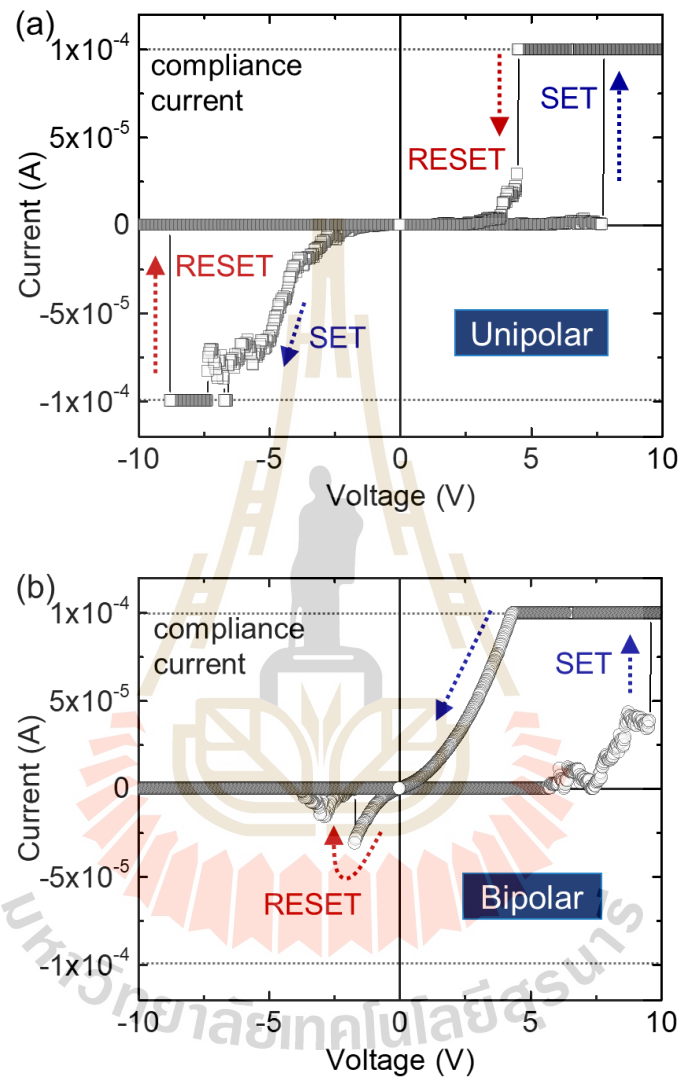


Figure 4.1 Typical I - V curve of single ZnO nanowire. The voltage was applied in the following sequence: 0 V to 10 V, 10 V to 0 V, 0 V to -10 V and -10 V to 0 V, at 0.025 V/s and compliance current of 0.1 mA. Both unipolar (a) and bipolar (b) behaviors were observed.

By sweeping voltage in both polarities, both unipolar (Figure 4.1(a)) and bipolar (Figure 4.1(b)) behaviors were observed in ZnO nanowire; however, 90% of obtained I - V characteristics exhibit the unipolar behavior. The unipolar behavior was studied by applying a only positive voltage on the tip. Figure 4.2 show a typical unipolar RS behavior of a single ZnO nanowire. By sweeping voltage from 0 to 10 V, at 0.025 V/s and a compliance current of 0.1 mA, we observed an abrupt increase of current at the $V_{\text{FORMING}} = 5.7$ V. The nanowire changes from the initial state to a LRS, called a forming process. When sweeping voltage from zero again, the nanowire remains in LRS, and the current drops at a $V_{\text{RESET}} = 1.7$ V. The nanowire changes to a HRS, called a reset process. The HRS can be switched to the LRS by applying the higher voltage $V_{\text{SET}} = 4.1$ V, called a set process, which has similar resistance as the forming process.

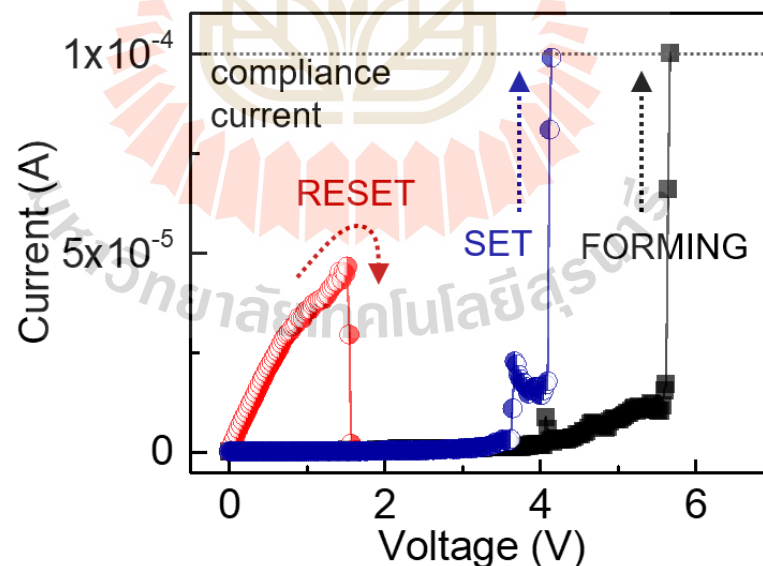


Figure 4.2 Typical unipolar RS behavior was observed by applying only positive voltage sweep with a compliance current 0.1 mA. The forming, reset and set processes are shown in black, red and blue curves.

The cycling endurance of ZnO NW-based memory devices was also studied. The RS is reproducible from cycle to cycle, as shown in Figure 4.3(a). One switching cycle is composed of a reset and a set processes (excluding the forming process). After forming, the V_{SET} and V_{RESET} of a nanowire over 5 switching cycles are show in Figure 4.3(b). The switching voltages varies for different switching cycles and overlap between reset and set ranges, which cause switching failure and still cannot be used to memory applications. The reset and the set processes should be repeated many switching cycles for memory applications. In our work, the cycling endurance is still limited due to the breakdown of nanowires under Joule heating.

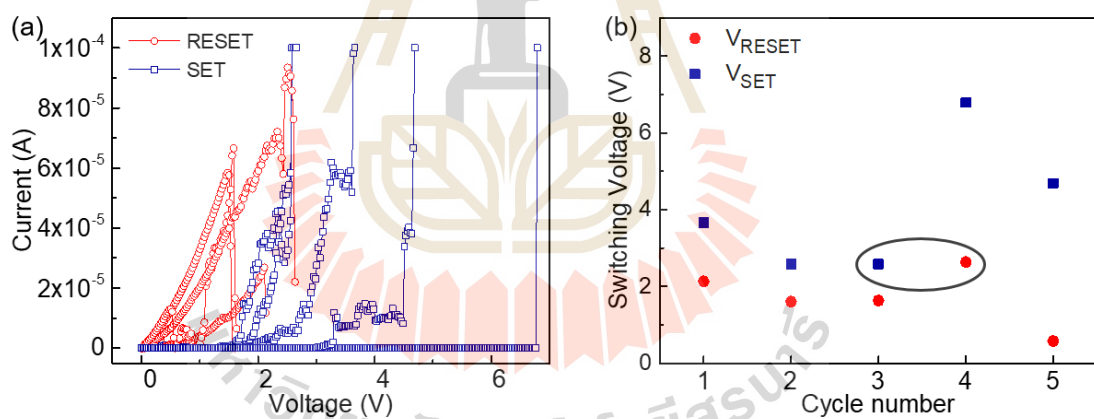


Figure 4.3 Repeated switching observed on a single ZnO nanowire. (a) The I - V curve of 5 switching cycles, (b) reset and set voltages distribution as a function of cycle's number.

By performing the measurement on an AFM platform, we are able to measure the I - V characteristics of many nanowires. Figure 4.4 shows the switching voltages distribution of 1st -cycle unipolar RS behavior that taken from 20 nanowires. On average $V_{FORMING} = 7 \pm 2$ V $>$ $V_{SET} = 4 \pm 2$ V $>$ $V_{RESET} = 3 \pm 2$ V. Large variations of the switching voltages suggest multiple conduction mechanisms, which will be discussed later.

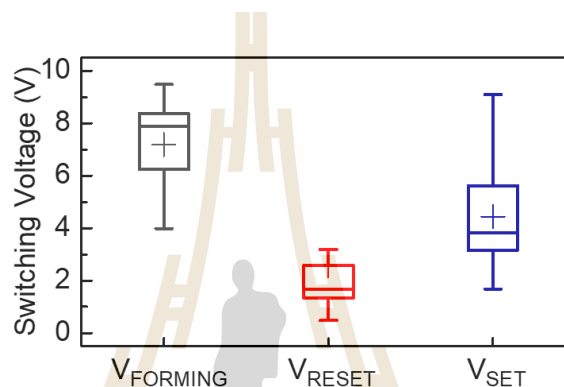


Figure 4.4 Box plot of $V_{FORMING}$, V_{RESET} , and V_{SET} taken from 20 nanowires. The crosses indicate the average value.

4.2 Conduction Mechanisms

RS behavior is characterized by different conduction mechanisms with unique I - V characteristics: Ohmic conduction ($I \propto V$), Schottky conduction ($\ln(I) \propto V^{1/2}$), Pool-Fenkel conduction ($\ln(I/V) \propto V^{1/2}$), trap-free space-charge-limited conduction (SCLC, $I \propto V^2$), as was described in section 2.4. These characteristics are found in both unipolar and bipolar RS systems. Most studies report Ohmic conduction for LRS. For the unipolar RS in our sample, however, the behavior of the LRS diversifies. Figure 4.5(a) shows I - V curves in double logarithmic scale from two reset processes of the same nanowire. For one cycle, the LRS shows Ohmic conduction, a linear I - V relationship

with slope ~ 1 until switching to the HRS. In another cycle however, the LRS exhibits Ohmic conduction at applied voltage < 0.7 V and SCLC with slope ~ 2.5 at higher voltage. The slope > 2 during SCLC is described as a trap-controlled SCLC (Chen et al., 2012; Kim et al., 2007; Lampert and Schilling, 1970). Presence of a trap-controlled process is not surprising since it is well-known that ZnO nanowires grown by the hydrothermal method contain defects (Greene et al., 2003). We emphasize that the change in the conduction behavior is not due to damaged conductive paths since we are still able to observe resistive switching behavior in the following switching cycles. Moreover, the behavior of the following cycles may exhibit Ohmic conduction or Ohmic+SCLC, independent of the previous cycles. Ohmic conduction occurs approximately 75% of the time. When comparing behaviors of the LRS from different nanowires, we also found the mixed behavior. Figure 4.5(b) plots I - V curves of the reset process of two nanowires with cross-section area $0.5 \mu\text{m}^2$ and $0.2 \mu\text{m}^2$. The $0.2 \mu\text{m}^2$ wire exhibits an Ohmic conduction while $0.5 \mu\text{m}^2$ wire shows Ohmic+SCLC behavior. Again, these wires still exhibit RS behavior in the following cycle; therefore, the mixed conduction behavior is not due to the filament damage.

The HRS conduction is similar for different cycles and nanowires during unipolar RS behavior. Figure 4.6 shows double logarithmic plots of the I - V curves from different nanowires during the set process. The I - V curves follow $I \propto V^n$ with different n values. At applied voltage < 0.3 V, we observed $n = 1.3 - 1.5$, obtained from the slope of the log-log plot, followed by a current drop. According to previous studies, this is still considered Ohmic conduction (Huang et al., 2013; Kukreja et al., 2009; Yoo et al., 2014). At applied voltage > 1 V, the current follows a power law with $n > 3$ before transitioning to the LRS. Such rapid increases in current is recognized as trap-controlled

SCLC (Chen et al., 2012; Kim et al., 2007; Lampert and Schilling, 1970). The trap-controlled SCLC is seen in both LRS and HRS, emphasizing the important roles of defects in these devices.

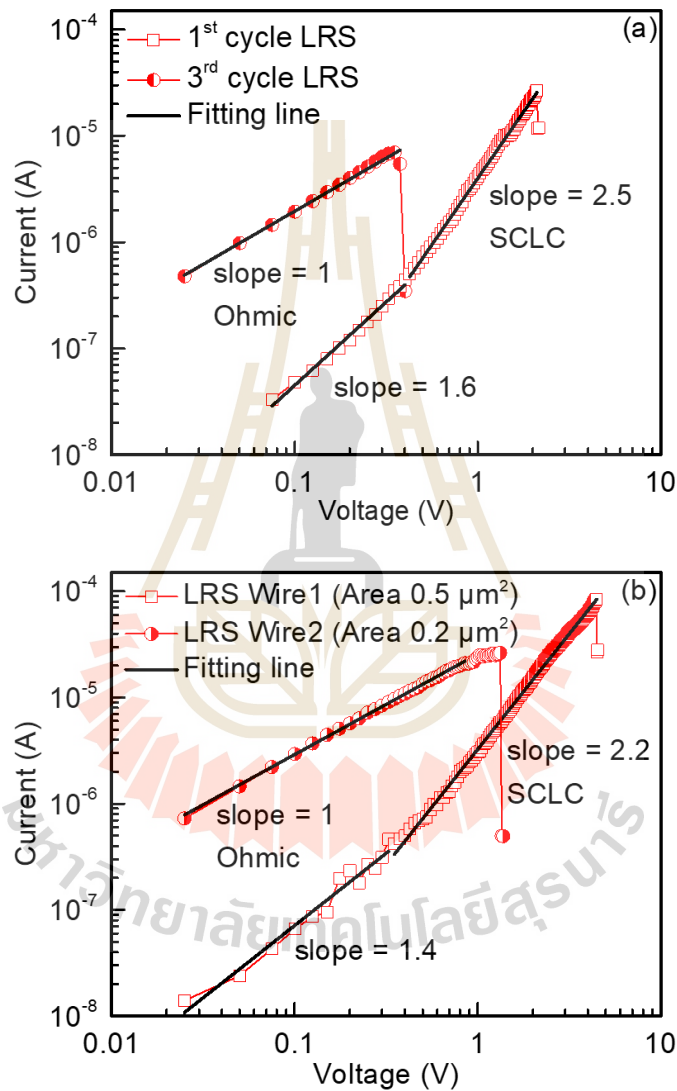


Figure 4.5 LRS I - V characteristics. (a) Two switching cycles of a single ZnO nanowire, and (b) of different nanowires in LRS showing Ohmic and SCLC conduction.

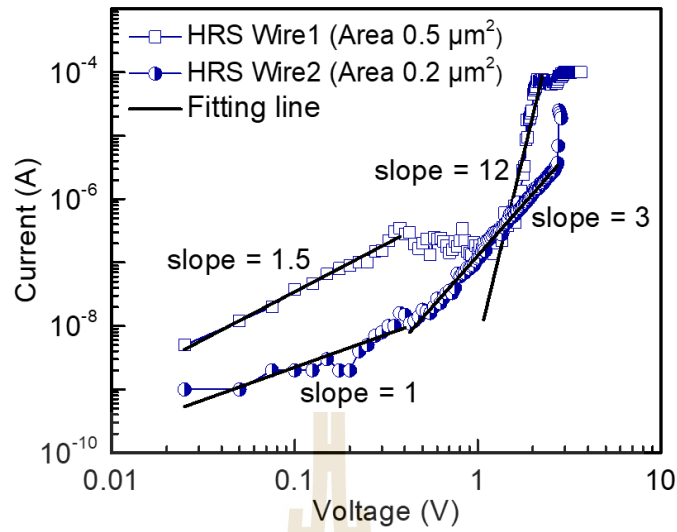


Figure 4.6 HRS I - V characteristics of two nanowires show Ohmic conduction at low voltage and SCLC conduction at high voltage.

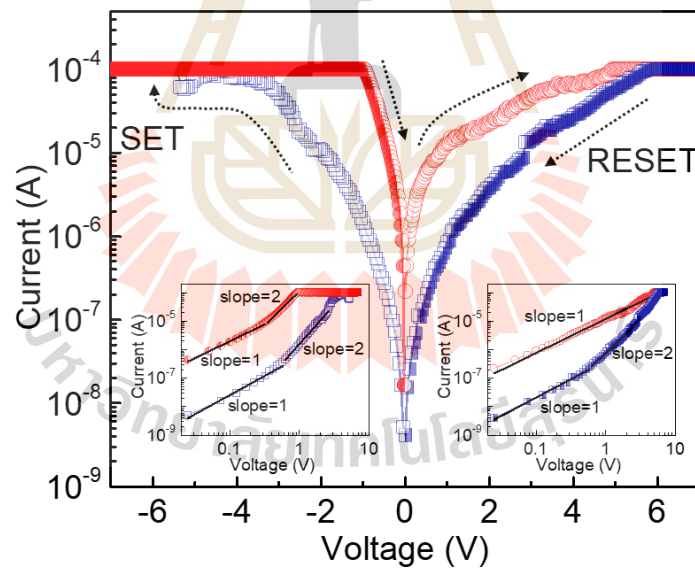


Figure 4.7 Typical I - V curve of bipolar RS behavior. The right (left) inset shows the positive (negative) voltage regime of the I - V curve in a log-log scale.

The conduction mechanism of bipolar switching was also discussed. Figure 4.7 shows some I - V characteristic of the bipolar RS behavior. The right (left) inset replots the positive (negative) voltage regime of the I - V curve in a double logarithmic plot. The LRS curves show a linear relationship with a slope of ~ 1 at applied voltage < 0.5 V, suggesting an Ohmic conduction, followed by a trap-free SCLC with slope ~ 2 . The I - V curve for the HRS is similar with higher resistance (lower current). Such conduction behavior is often attributed to the formation and rupture of conductive filaments (Lee et al., 2009). After the rupture, transport is through the remaining filaments.

4.3 Size-independence I - V Characteristics

Such mixed conduction behavior suggests multiple conduction paths with different conduction mechanisms. In some ZnO nanowire-based memory devices, the RS behavior is attributed to conduction at the surface (Chiang et al., 2011; Yang et al., 2011) or through wires (Qi et al., 2013). Such behavior is often size-dependent. By performing the measurement on an AFM platform, we can correlate the I - V characteristics of a nanowire to its cross-section area. Figure 4.8(a) shows the resistance of the LRS as a function of the nanowire cross-section area. The resistance values are independent of the nanowire size. The LRS with only Ohmic conduction often has lower resistance (order of $10^4 \Omega$ at 0.5 V) than those that exhibit Ohmic+SCLC behavior (order of $10^6 \Omega$ at 0.5 V). Because the resistance of the HRS state is similar, the LRS state with Ohmic conduction thus has a higher on-off ratio (~ 3 orders of magnitude), as shown in Figure 4.8(b). Since the conduction does not depend on the size of the nanowires, we attribute the two behaviors to different types of conductive filaments: the Ohmic conduction is due to defect-free Ag-based filaments and the

Ohmic+SCLC conduction is due to oxygen vacancies-based filaments (Lee et al., 2010). Our results indicate that different types of conduction mechanisms can coexist in the same nanowire, with different resistance values and on-off ratios.

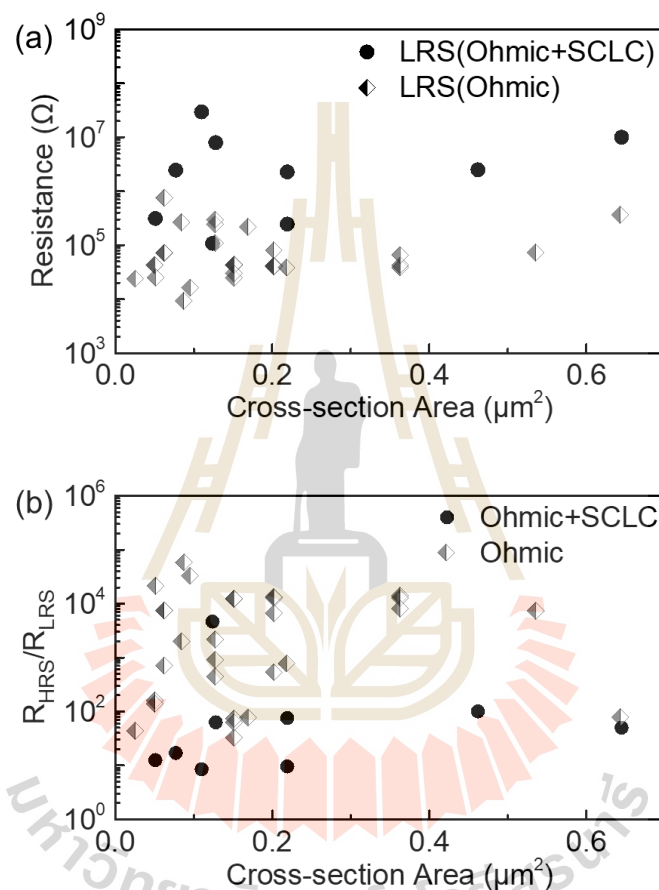


Figure 4.8 The resistance of unipolar RS behavior as a function of the nanowire cross-section area. (a) Distribution of Ohmic and SCLC behaviors and (b) on-off ratio for different nanowire cross-sections.

To further elaborate on the size-independent behavior, we looked at the switching voltages during the unipolar RS as a function of the cross-section area (Figure

4.9). We observed no significant correlation between the switching voltage and the cross-section area of the nanowire. If the RS behavior is due to the homogenous motion of carriers at the interface, size-dependent behavior would be expected. This analysis further supports the filament-based model being the underlying mechanism.

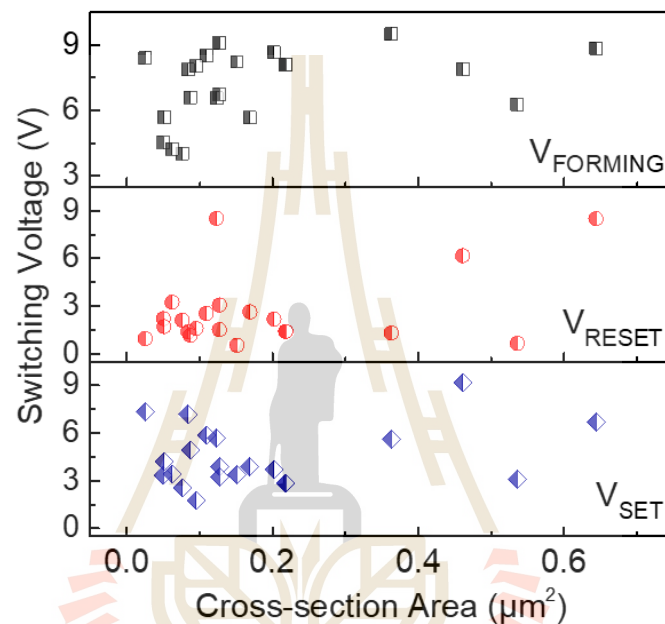


Figure 4.9 Box plot of $V_{FORMING}$, V_{RESET} , and V_{SET} taken from 20 nanowires. The crosses indicate the average value.

4.4 *I-V* Characteristics of Sm-substituted BFO

In order to ensure the accurate *I-V* measurement, C-AFM was also used to study *I-V* characteristics of Sm-substituted BFO. The voltage was applied to the BFM sample. Figure 4.10(a) shows the hysteresis loop in *I-V* curve of Sm 5%-BFO. The *I-V* characteristic can be measured even the current is very small (is in the order of nA). Moreover, the conduction mechanism of BFO was also studied by curve fitting. Figure 4.10(b) and (c) show forward *I-V* curve in semi-logarithmic and double logarithmic

scales with the fitting lines. At the low voltage region, I - V curve shows the Schottky conduction, whereas the SCLC dominates in the high voltage region.

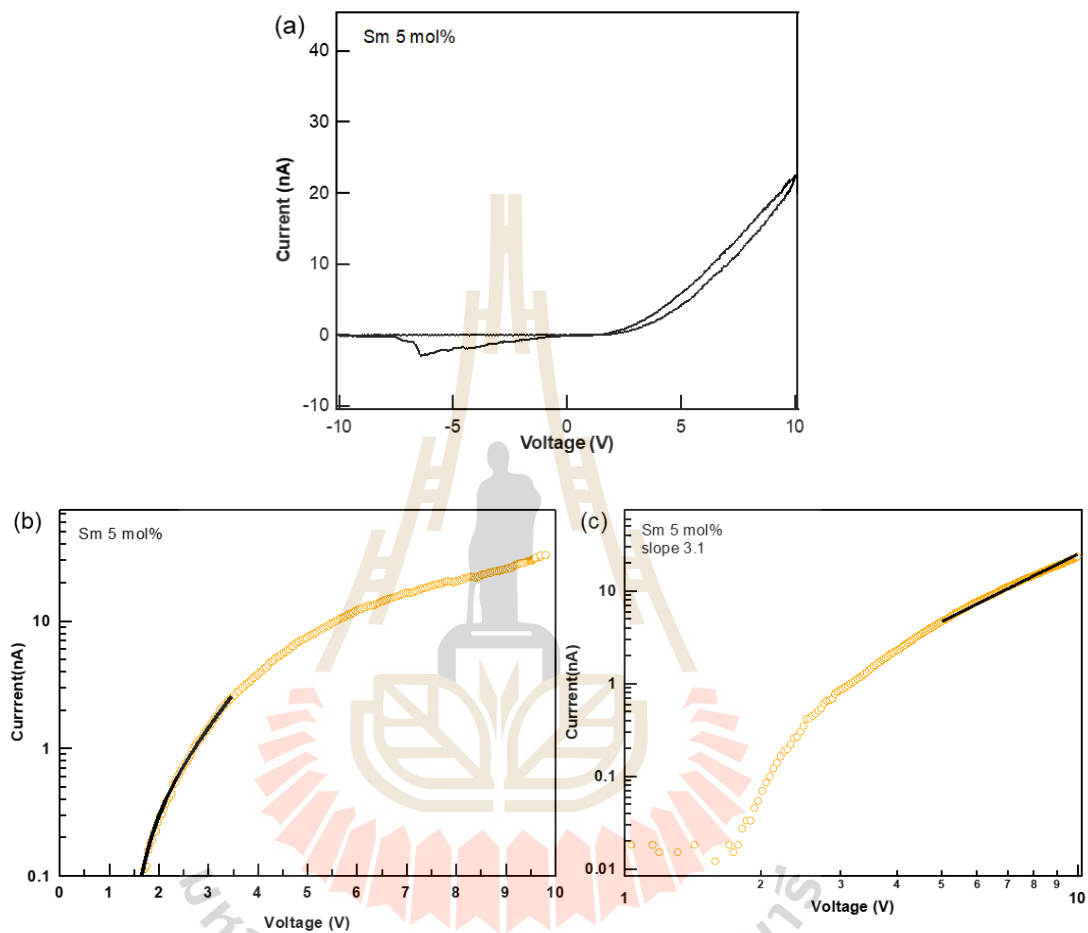


Figure 4.10 (a) Typical hysteresis loop in I - V curve of Sm 5%-BFO measured by C-AFM. (b) The forward I - V curve with Schottky model fitting (black curve) and (c) SCLC model fitting.

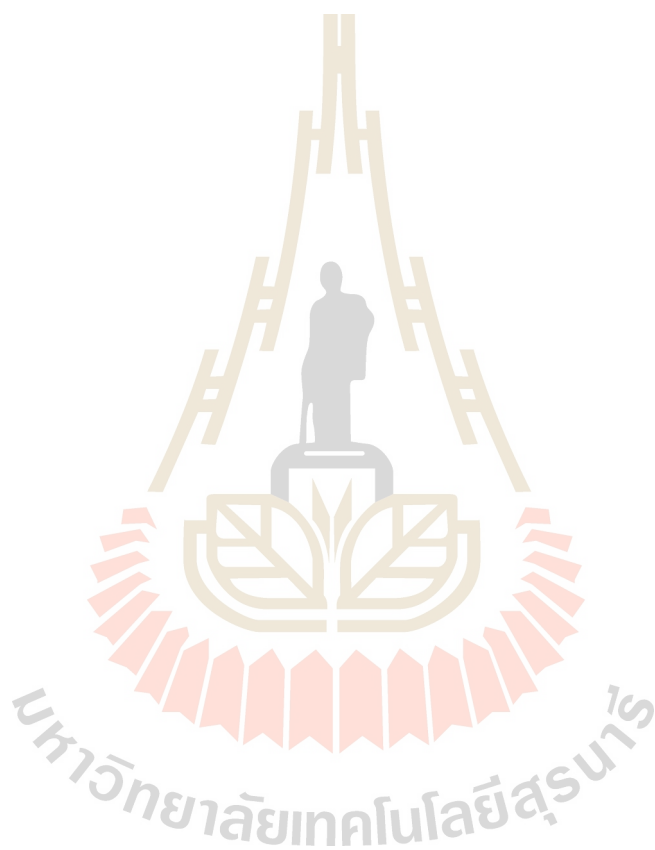
CHAPTER V

CONCLUSIONS

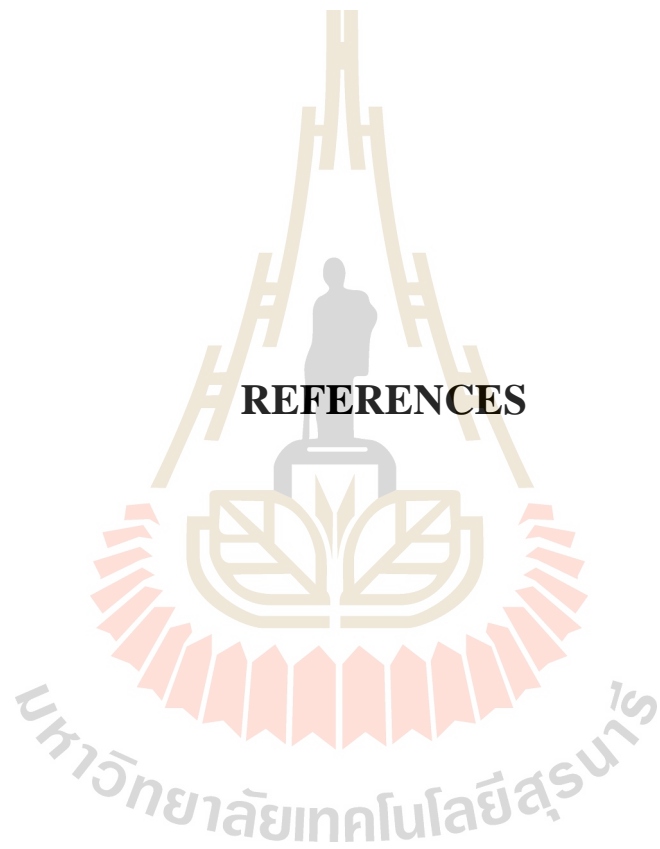
In summary, the RS behavior of n-type ZnO nanowires was successfully investigated by C-AFM. ZnO nanowires were grown vertically on a Ag/glass substrate using a seed-assisted hydrothermal process. The Ag substrate and the AFM probe serve as the bottom and the top electrode for *I-V* characteristic measurements. The AFM platform allows access to individual nanowire and studied the size-dependent behavior of different nanowires. We found the existence of both unipolar and bipolar RS behavior in ZnO nanowires. Most nanowires exhibited unipolar RS behavior, but occasionally bipolar RS behavior was observed. For unipolar type, the RS behaviors are independent of the nanowire sizes, indicating that the RS is filament-based. The LRS during unipolar switching may exhibit Ohmic or Ohmic+SCLC conduction. The former with lower resistance, is likely metallic-based filaments, while the latter with higher resistance is likely oxygen vacancy-based filaments.

Such defect-based conductive paths are often shortened by the lower resistance defect-free path in larger devices. In nanoscale devices like the nanowire, the number of conduction paths is limited and understanding defect-based conduction can be the key for reducing variation in RRAM performance and increasing the on-off ratio. Such behavior is not visible with a macroscopic measurement and is only revealed with C-AFM measurements of individual nanowires.

We believe that our research will serve as a base for future studies on ZnO nanowire-array-based memory. By using microscopic probes to read and write the data, ZnO nanowires is a promising candidate for improvement the limited array size.



REFERENCES



REFERENCES

- Chae, S. C., Lee, J. S., Kim, S., Lee, S. B., Chang, S. H., Liu, C., and Noh, T. W. (2008). Random circuit breaker network model for unipolar resistance switching. **Advanced Materials**. 20(6): 1154–1159.
- Chang, W.-Y., Lai, Y.-C., Wu, T.-B., Wang, S.-F., Chen, F., and Tsai, M.-J. (2008). Unipolar resistive switching characteristics of ZnO thin films for nonvolatile memory applications. **Applied Physics Letters**. 92(2): 022110.
- Chen, C., Pan, F., Wang, Z. S., Yang, J., and Zeng, F. (2012). Bipolar resistive switching with self-rectifying effects in Al/ZnO/Si structure. **Journal of Applied Physics**. 111(1).
- Chen, J. Y., Hsin, C. L., Huang, C. W., Chiu, C. H., Huang, Y. T., Lin, S. J., and Chen, L. J. (2013). Dynamic evolution of conducting nanofilament in resistive switching memories. **Nano Letters**. 13(8): 3671–3677.
- Chiang, Y. De, Chang, W. Y., Ho, C. Y., Chen, C. Y., Ho, C. H., Lin, S. J., and He, J. H. (2011). Single-ZnO-nanowire memory. **IEEE Transactions on Electron Devices**. 58(6): 1735–1740.
- Cui, J. (2012). Zinc oxide nanowires. **Materials Characterization**. 64: 43–52.
- Greene, L. E., Law, M., Goldberger, J., Kim, F., Johnson, J. C., Zhang, Y., and Yang, P. (2003). Low-Temperature Wafer-Scale Production of ZnO Nanowire Arrays. **Angewandte Chemie International Edition**. 42(26): 3031–3034.

- Huang, C. H., Huang, J. S., Lai, C. C., Huang, H. W., Lin, S. J., and Chueh, Y. L. (2013). Manipulated transformation of filamentary and homogeneous resistive switching on ZnO thin film memristor with controllable multistate. **ACS Applied Materials and Interfaces**. 5(13): 6017–6023.
- Huang, Y., Luo, Y., Shen, Z., Yuan, G., and Zeng, H. (2014). Unipolar resistive switching of ZnO-single-wire memristors. **Nanoscale Research Letters**. 9(1): 1–5.
- Kasamechonchung, P., Horprathum, M., Boonpavanitchakul, K., Supaka, N., Prompinit, P., Kangwansupamonkon, W., and Klamchuen, A. (2015). Morphology-controlled seed-assisted hydrothermal ZnO nanowires via critical concentration for nucleation and their photoluminescence properties. **Physica Status Solidi (A)**. 212(2): 394–400.
- Kim, K. M., Choi, B. J., Shin, Y. C., Choi, S., and Hwang, C. S. (2007). Anode-interface localized filamentary mechanism in resistive switching of TiO₂ thin films. **Applied Physics Letters** 91(1): 3–6.
- Kim, K. M., Jeong, D. S., and Hwang, C. S. (2011). Nanofilamentary resistive switching in binary oxide system; A review on the present status and outlook. **Nanotechnology**. 22(25).
- Kukreja, L. M., Das, A. K., and Misra, P. (2009). Studies on nonvolatile resistance memory switching in ZnO thin films. **Bulletin of Materials Science**. 32(3): 247–252.
- Lampert, M. A., and Schilling, R. B. (1970). Current injection in solids: The regional approximation method. In **Semiconductors and Semimetals**. New York: Academic Press.

- Lanza, M. (2014). A review on resistive switching in high-k dielectrics: A nanoscale point of view using conductive atomic force microscope. **Materials**. 7(3): 2155–2182.
- Lee, J. S., Lee, S., and Noh, T. W. (2015). Resistive switching phenomena: A review of statistical physics approaches. **Applied Physics Reviews**. 2(3).
- Lee, S., Kim, H., Park, J., and Yong, K. (2010). Coexistence of unipolar and bipolar resistive switching characteristics in ZnO thin films. **Journal of Applied Physics**. 108(7): 2008–2011.
- Lee, S., Kim, H., Yun, D.-J., Rhee, S.-W., and Yong, K. (2009). Resistive switching characteristics of ZnO thin film grown on stainless steel for flexible nonvolatile memory devices. **Applied Physics Letters**. 95(26): 262113.
- Qi, J., Olmedo, M., Zheng, J. G., and Liu, J. (2013). Multimode resistive switching in single ZnO nanoisland system. **Scientific Reports**. 3: 1–6.
- Raffone, F., Risplendi, F., and Cicero, G. (2016). A New Theoretical Insight into ZnO NWs Memristive Behavior. **Nano Letters**. 16(4): 2543–2547.
- Sawa, A. (2008). Resistive switching in transition metal oxides. **Materials today**. 11(6): 28–36.
- Schmidt-Mende, L., and MacManus-Driscoll, J. L. (2007). ZnO - nanostructures, defects, and devices. **Materials Today**. 10(5): 40–48.
- Simanjuntak, F. M., Panda, D., Wei, K. H., and Tseng, T. Y. (2016). Status and prospects of ZnO-based resistive switching memory devices. **Nanoscale research letters**. 11(1): 368.
- Sze, S. M. and Ng, K. K. (2006). **Physics of Semiconductor Devices**. 3rd Edition, Hoboken: John Wiley & Sons.

- Waser, R., and Aono, M. (2007). Nanoionics-based resistive switching memories. **Nature Materials**. 6(11): 833–840.
- Yang, Y., Zhang, X., Gao, M., Zeng, F., Zhou, W., Xie, S., and Pan, F. (2011). Nonvolatile resistive switching in single crystalline ZnO nanowires. **Nanoscale**. 3(4): 1917–1921.
- Yoo, E. J., Shin, I. K., Yoon, T. S., Choi, Y. J., and Kang, C. J. (2014). Resistive Switching Characteristics of ZnO Nanowires. *Journal of Nanoscience and Nanotechnology*. 14(12): 9459–9464.
- Zhuge, F., Peng, S., He, C., Zhu, X., Chen, X., Liu, Y., and Li, R. W. (2011). Improvement of resistive switching in Cu/ZnO/Pt sandwiches by weakening the randomness of the formation/rupture of Cu filaments. **Nanotechnology**. 22(27).
- Zhuge, F., Li, K., Fu, B., Zhang, H., Li, J., Chen, H., and Luo, H. (2015). Mechanism for resistive switching in chalcogenide-based electrochemical metallization memory cells. **AIP Advances**. 5(5).
- Zhang X. G. (1996). **Corrosion and Electrochemistry of Zinc**. New York: Springer.

CURRICULUM VITAE

Name Ms. Oradee Srikimkaew
Born August 22th, 1994 in Buriram, Thailand
Citizenship Thai
Address 47/1 M.1, Sumrongmai, Lahan Sai, Buriram, 31170, Thailand
E-mail oradee.sw@gmail.com

Education

2013-2016 B.Sc. (Physics), Suranaree University of Technology, Thailand
2017-present M.Sc. (Physics), Suranaree University of Technology, Thailand

Poster presentation:

Riou, C., Cordeiro, L., Chaiyasitdhi, A., Srikimkaev, O., Suebka, S., Nadal-Desbarats, L., Kundhikanjana, W., Gérard, N. (2018). Motility and atomic force microscopy observation of avian spermatozoa incubated in uterine fluid. Presented at 34th Scientific Meeting of the AETE, Nantes, FRA (2018-09-07 - 2018-09-08).

Srikimkaev, O., Suebka, S., Kundhikanjana, W. (2017). Study of the Resistive Switching Behavior in ZnO Nanowires Using Atomic Force Microscope. Presented at The Conference on Science and Technology for Youths, Bangkok International Trade & Exhibition Centre: BITEC, Thailand (2017-06-03 - 2017-06-04).